ktu
1922

Kaunas University of Technology

Faculty of Mechanical Engineering and Design

Research of Structures with Embedded Sensors

Master's Final Degree Project

Justinas Balodis

Project author

Assoc. prof. Marius Rimašauskas

Supervisor

Kaunas, 2023

Kaunas University of Technology

Faculty of Mechanical Engineering and Design

Research of Structures with Embedded Sensors

Master's Final Degree Project

Mechatronics (6211EX017)

Justinas Balodis

Project author

Assoc. prof. Marius Rimašauskas

Supervisor

Lect. Tomas Kuncius

Reviewer

Kaunas, 2023

Kaunas University of Technology

Faculty of Mechanical Engineering and Design

Justinas Balodis

Research of Structures with Embedded Sensors

Declaration of Academic Integrity

I confirm the following:

1. I have prepared the final degree project independently and honestly without any violations of the copyrights or other rights of others, following the provisions of the Law on Copyrights and Related Rights of the Republic of Lithuania, the Regulations on the Management and Transfer of Intellectual Property of Kaunas University of Technology (hereinafter – University) and the ethical requirements stipulated by the Code of Academic Ethics of the University;

2. All the data and research results provided in the final degree project are correct and obtained legally; none of the parts of this project are plagiarised from any printed or electronic sources; all the quotations and references provided in the text of the final degree project are indicated in the list of references;

3. I have not paid anyone any monetary funds for the final degree project or the parts thereof unless required by the law;

4. I understand that in the case of any discovery of the fact of dishonesty or violation of any rights of others, the academic penalties will be imposed on me under the procedure applied at the University; I will be expelled from the University and my final degree project can be submitted to the Office of the Ombudsperson for Academic Ethics and Procedures in the examination of a possible violation of academic ethics.

Justinas Balodis

Confirmed electronically

Kaunas University of Technology

Faculty of Mechanical Engineering and Design

Task of the Master's Final Degree Project

Given to the student – Justinas Balodis

1. Title of the Project

Research of Structures with Embedded Sensors
(In English)

Konstrukcijų su įterptiniais jutikliais tyrimas
(In Lithuanian)

2. Aim and Tasks of the Project

Aim: to develop and investigate 3D printed structure with integrated sensors for mechanical properties evaluation.
Tasks:
1. to develop methodology for manufacturing of structures with embedded sensors;
2. to evaluate the impact of sensors on mechanical properties of structures;
3. to evaluate mechanical behaviour of 3D printed structures under static and dynamic loading;
4. to perform economic analysis including materials, equipment, labour expenses.

3. Main Requirements and Conditions

Developed 3D printed samples with main functions implemented. Sample test plan prepared and implemented. Strain measurement equipment and process defined. Analysis of data gathered presented with conclusions.

4. Additional Requirements for the Project, Report and its Annexes

"Not applicable"

Project author	Justinas Balodis		2023.03.03
	(Name, Surname)	*(Signature)*	*(Date)*
Supervisor	Marius Rimašauskas		2023.03.03
	(Name, Surname)	*(Signature)*	*(Date)*
Head of study field programs	Regita Bendikienė		2023.03.03
	(Name, Surname)	*(Signature)*	*(Date)*

Summary

Since the patent of the strain gauge design, this invention started to shape the world we knew before and increased the availability of the strain measurement in different applications. Having this in mind we various application of the strain gauge were found in industries. Nowadays in engineering strain measurement is important field to study. In this paper the idea of the embedded strain gauges are analysed and discussed, as far as industry sees the need of it with upcoming additive manufacturing to all industries, and applications from the rapid prototyping till the aerospace industries. In order to get constant data on structure health and resistance, the strain gauges with data acquisition system can be used. This assures the real time and constant flow of data to keep the structure in safe mode. In order to get the data, the strain gauges must be installed, the installation usually takes time and costs, and also in some cases, when it comes to aggressive environments the upkeep and supervision is complicated. In such cases the embedded sensors including strain gauges would be helpful. In this research paper there is an overview of different strain measurement methods is done and based on all observations, decision was made to proceed with integration of sophisticated strain gauge with ability to withstand elevated temperatures. The temperature resistance is needed, because during 3D printing, temperature reaches more than 200° Celsius. Strain gauges were prepared and embedded in the specimens produced using the PLA as main structure material. After the production and validation of resistance level on each of strain gauge, the data acquisition system was built on the base of Arduino minicomputer to represent and to log the test results and data. For the tests there were two direction chosen, one part of the tests were done using special test bench built and second part was the validation of strain measurement on the test machine.

Santrauka

Patentavus įtempimų jutiklio dizainą, šis išradimas pradėjo keisti mums anksčiau pažįstamą pasaulį ir padidino deformacijų matavimo prieinamumą įvairiose srityse. Turint tai omenyje, pramonės šakose buvo rasta įvairių deformacijų jutiklių pritaikymų. Šiais laikais inžinerijos srityje deformacijų matavimas yra svarbi studijų sritis. Šiame darbe analizuojama ir aptariama įterptųjų deformacinių matuoklių idėja, nes įvairios pramonės sritys mato, kad tai reikalinga su visose pramonės šakose ir galimas pritaikymais nuo greito prototipų kūrimo iki aviacijos ir kosmoso pramonės. Norint gauti nuolatinius duomenis apie konstrukcijos būklę ir atsparumą, galima naudoti deformacijų jutiklius su duomenų rinkimo sistema. Tai užtikrina nuolatinį duomenų srautą realiu laiku ir padeda struktūrą išlaikyti tinkamą eksploatacijai. Norint gauti duomenis, reikia sumontuoti deformacinius matuoklius, montavimas dažniausiai užtrunka ir kainuoja, o kai kuriais atvejais, kai kalbama apie agresyvią aplinką, jų priežiūra yra sudėtinga. Tokiais atvejais įterptieji jutikliai, įskaitant deformacijos matuoklius, yra nepakeičiamai naudingi. Šiame darbe apžvelgiami įvairūs deformacijų matavimo metodai ir išanalizavus juos buvo priimtas sprendimas integruoti sudėtingą į konstrukciją jutklį, galintį atlaikyti aukštą temperatūrą. Atsparumas temperatūrai reikalingas, nes 3D spausdinimo metu temperatūra siekia daugiau nei 200°C. Įtempimo jutikliai buvo paruošti ir įterpti į bandinius, pagamintus naudojant PLA kaip pagrindinę konstrukcijos medžiagą. Sukūrus ir patvirtinus kiekvieno įtempio jutiklio varžos lygį, Arduino mini kompiuterio pagrindu buvo sukurta duomenų rinkimo sistema, skirta bandymų rezultatams ir duomenims registruoti. Bandymams buvo pasirinktos dvi kryptys, viena bandymų dalis buvo atlikta naudojant specialų bandymų stendą, o antroji dalis buvo įtempių matavimo bandymo mašinoje patvirtinimas.

Table of Contents

List of Figures

List of Tables

List of Abbreviations and Terms

Abbreviations:

PDMS   – Polydimethylsiloxane foam;
FSR   – force sensitive resistor;
FDM   – Fused Deposition Modelling;
FBG   – Fiber Bragg grating;
ABS   – Acrylonitrile Butadiene Styrene;
AJP   – Aerosol jet printing.
IDE   – Interdigitated electrode
CSG   – Capacitance based strain gauge
DAQ   – Data Acquisition System

Terms:

Additive manufacturing – is a process of creating three-dimensional objects by adding material layer by layer. It uses computer-aided design (CAD) software and various materials such as plastics, metals, and ceramics to build complex shapes that would be difficult or impossible to produce with traditional manufacturing methods.

Introduction

Additive manufacturing technology has revolutionized the way products are designed and manufactured. Integration of strain sensors in 3D printing adds a new dimension of capabilities to the technology. Significance of 3D printing with integrated strain sensors provides several benefits for the industry, e.g. quality control with the use of integrated strain sensors, it is possible to monitor the quality and consistency of the 3D printing process. The sensors can detect any flaws or defects in the printing process, which can help manufacturers to take corrective actions. Moreover the structural health monitoring, when the 3D printed objects with integrated strain sensors can be used for structural condition monitoring, where the sensors can detect any changes in the structural integrity of the object. This can be particularly useful in fields like aerospace and civil engineering, where the safety and durability of structures are critical. In the recent year the increase of research of the smart devices in healthcare segment is significant, in some of research papers [1] examples presented where simples smartphones used to support experiments. Keeping this in mind the 3D printing with integrated strain sensors can be used to create smart devices that can detect and respond to changes in their environment and send the data to the smartphone. For example, a prosthetic limb with strain sensors can detect the movement of the human muscles and respond accordingly. Moreover the use of integrated strain sensors in 3D printing can also improve the efficiency of the manufacturing process. By monitoring the strain on the printed object during the printing process, it is possible to optimize the printing parameters and reduce material waste. Overall, the integration of strain sensors in 3D printing has significant potential to enhance the quality, safety and efficiency of manufactured products, as well as enable the creation of innovative new devices and applications. The variance of 3D printing technologies refers to the diversity and range of different 3D printing methods [2], materials and applications that exist. There are many different types of 3D printing technologies, each with its own strengths and weaknesses. Some of the most common 3D printing technologies include: Fused Deposition Modelling - this is the most widely used 3D printing technology. FDM involves heating a thermoplastic filament and extruding it through a nozzle to build up layers. Stereolithography is a technique that builds an item layer by layer by curing a liquid resin with a laser. There are also many different materials that can be used in 3D printing, including plastics, metals, ceramics and even biological materials. The applications of 3D printing are also varied and wide-ranging, including prototyping, product design, engineering, medical applications and more. Overall, the variance of 3D printing technologies reflects the incredible diversity of possibilities that 3D printing offers. As the technology continues to evolve and improve, we can expect even more innovative and exciting applications to emerge. Additive manufacturing can be a useful tool in the production of solar cells, especially for creating complex and customized designs. Here are a few ways that 3D printing is being used in solar cell production, it can be used to create custom moulds for the fabrication of solar cells. These moulds can be designed to match the desired shape and size of the final product, allowing for greater flexibility and precision in the manufacturing process. Also prototyping and testing: 3D printing can be used to quickly create prototypes of new solar cell designs. This allows researchers and manufacturers to test different configurations and materials without the need for expensive and time consuming traditional manufacturing methods. Moreover 3D printing can be used to create components such as brackets, mounts and connectors for solar panels. These parts can be custom-designed to fit specific installations and environments and can be produced quickly and affordably using 3D printing technology. Overall, 3D printing has the potential to revolutionize the way that solar cells are manufactured and designed, making the process more efficient, cost effective and sustainable [3].

Aim: to develop and investigate 3D printed structure with integrated sensors for mechanical properties evaluation.

Tasks:
1. to develop methodology for manufacturing of structures with embedded sensors;
2. to evaluate the impact of sensors on mechanical properties of structures;
3. to evaluate mechanical behaviour of 3D printed structures under static and dynamic loading;
4. to perform economic analysis including materials, equipment, labour expenses.

Hypothesis: 3D printed structures with integrated sensors can be embedded directly into 3D printed structures during the printing process, resulting a more efficient manufacturing process.

1. Overview of 3D/4D Printed Structures and Structures with Embedded Sensors

Over the past 20 years, the internet has spurred a technological boom, making innovative technologies more accessible and easier to use across various industries. This has disrupted traditional manufacturing systems and paved the way for the emergence of Industry 4.0. Central to this transformation is data, with more than 2.5 quintillion bytes of data generated daily and nearly 90% of all the data produced in just the last two years [4]. This brings new challenges and new opportunities for the all industries to have more various sensors embedded in the diverse constructions and structures, starting by structural health monitoring in civil engineering or sensors used in aerospace industries where the structure health is vital element to follow during the lifecycle of the system. Various embedded sensors can give significant impact for the healthcare industries in order to keep data flow on patient condition and recovery. In medicine the 3D printed implants are already known ad used widely in numerous cases e.g. when bone tissue is missing or needed to be replaced. Sveral bone tissue replacement cases described by Korean researchers from Yonsei university [5], when the each patient specific skull deformity was properly accommodated by the 3D printed titanium implants, leaving no empty space. The surgical site recovered without any issues and postoperative computer tomography scans verified that the implants were positioned correctly. They concluded that 3D titanium implant may be the best source material for calvarial reconstruction in this case. The implant was produced in 2 mm thickness and achieved the same properties as human skull bone. Integrated sensors play a crucial role in the field of robotics by providing the necessary information for robots to perform tasks with greater accuracy, efficiency and safety. These sensors can detect various environmental factors such as temperature, humidity, pressure and light intensity, as well as indicate and quantify the proximity and position of objects. By incorporating this information into their decision making processes, robots can adapt to changing environments and conditions, avoid collisions and execute tasks with greater precision and accuracy. Furthermore, integrated sensors in robotics also enable the monitoring of robot performance and maintenance needs, allowing for timely repairs and reducing downtime. This ultimately leads to increased productivity, reduced costs and improved safety in various industries, such as manufacturing, healthcare and transportation. Overall, integrated sensors are essential for enhancing the capabilities and performance of robotics and enabling them to perform complex tasks in diverse settings. In this area the 4D printing is an advanced manufacturing technology that uses 3D printing to create objects that can transform or self-assemble over time in response to external stimuli. In other words, 4D printed objects have the ability to change their shape or functionality after they have been printed, adding an additional dimension of time to the manufacturing process. The process of 4D printing involves using materials that can respond to different stimuli, such as heat, light, water, or pressure, to activate shape-changing or self-assembling behaviour. These materials are typically designed to respond to specific stimuli in a controlled way, allowing them to deform, fold, or bend in specific ways. One of the main advantages of 4D printing is its potential to reduce manufacturing costs and increase efficiency by allowing objects to self-assemble or transform in response to external conditions. For example, 4D printed structures could be used in applications such as aerospace, construction, or medicine to create self-assembling structures that can adapt to changing environmental conditions or repair themselves when damaged. Overall, 4D printing is an exciting new field that is interesting for the future of manufacturing, design and engineering. While it is still in the early stages of development, the potential applications of this technology are vast and could revolutionize the way we think about creating and using objects in a wide range of industries. Strain sensors are commonly used in the aerospace industry to measure and monitor the strain or

deformation of various components and structures. These sensors can be used to detect changes in load or stress on critical parts, such as wings, fuselage, and engine components. The data collected by strain sensors is essential in ensuring the safety and reliability of aerospace systems. E.g. strain sensors are used to measure the load and strain on the wings of an aircraft during flight. This data is used to optimize the design of the wings and to detect any anomalies or damage that could affect the structural integrity of the aircraft. Moreover sensors can be used to monitor the deformation of engine components such as fan blades, turbine blades and bearings. This data is used to detect any changes in the mechanical properties of these components, which could lead to failure or damage. Overall, strain sensors are an essential component in the aerospace industry, providing critical data that is used to ensure the safety and reliability of aircraft and spacecraft.

Researchers from Jiangnan university published the paper [6] where they discusses the development of a dual security solution for robotic grippers, which combines closed loop force control and stress buffering capability. Scientists design and fabricate an integrated force sensitive smart polydimethylsiloxane (PDMS) foam, which contains an embedded force sensitive resistor (FSR) using 3D printing technology, shown on Fig.1. As seen from the design provided the pressure sensitive layer is covered in several conductive and insulation covers.
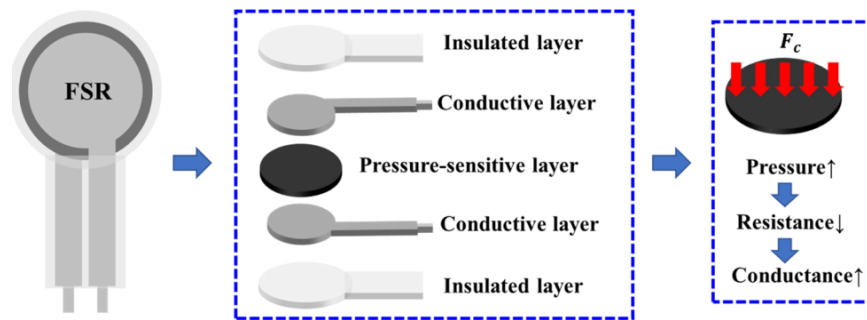
Fig. 1. Schematic design overview and working principle of FSR [6]

Real-time force measurement is transmitted back into the control loop with proportional integral rectification to accurately manage the driving air pressure. The PDMS foam structure offers a continuous stress buffer to absorb possible impact energy. The goal of this research is to improve the reliability of gripping applications, particularly for fragile objects, which are challenging to handle using conventional grippers. The dual security gripper with smart PDMS foam, which is detailed in Fig.2. is capable of precisely controlling the applied force and reliably gripping fragile objects even in the presence of disturbances.
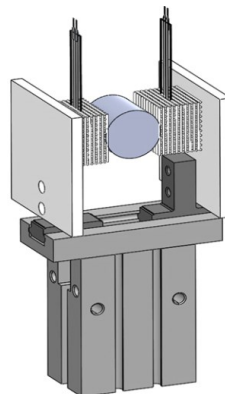
Fig. 2. 3D model of FSR sensors installed on the gripper [6]

The stress buffering capability of the PDMS foam structure provides an additional layer of protection against potential damage caused by collisions, working principle schematics is shown in Fig.3.
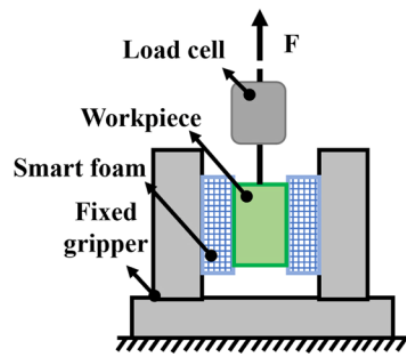
Fig. 3. Schematic diagram of robotic gripper enhanced with smart foam with embedded pressure sensors [6]

The results of the experiments demonstrate that the dual security gripper with smart PDMS foam is effective in enhancing the reliability of gripping applications. The researchers anticipate that this technology could be used in a wide range of applications including industrial automation, healthcare, aerospace and household robotics.

Study [7] made by Taiwanese university describes the development of an FBG-based one dimensional shock accelerometer using Fused Deposition Modelling (FDM) technology. The sensor consists of a bare fiber Bragg grating (FBG) fixed to a 3D printed elastomer structure seen in Fig.4., and the dimension of the sensor was simulated using finite element analysis shown in Fig.5. to explore its customizability. The deformation in the elastic material structure results in a change in the wavelength of the FBG sensor, which is used to measure acceleration. The results of the experiments demonstrate that the proposed FBG acceleration sensor is capable of measuring accelerations in the range of 655 g to 2635 g with a sensitivity of 1.16 pm/g, and the linear analysis shows that the linear values of the data obtained in the experiments are above 96%. The proposed FBG acceleration sensor is based on 3D printing technology, which provides several advantages such as fast manufacturing time, saving production costs and the ability to easily customize the size, weight and material of the structure. The sensor's operating frequency ranges from 200 to 3000 Hz, making it suitable for a wide range of applications.
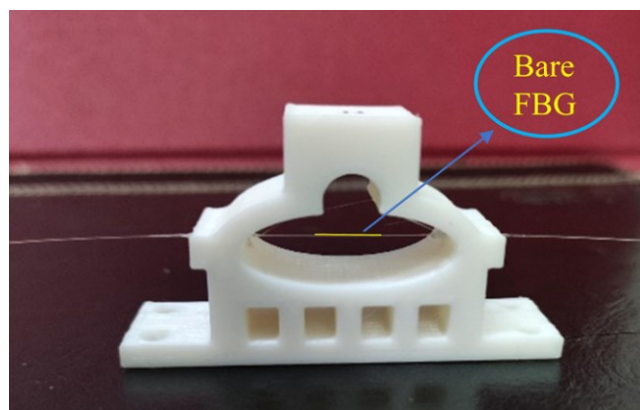
Fig. 4. The completed 3D printed sensor structure [7]

Additionally, the FBG accelerometer and the accelerometer signal acquired from the piezoelectric accelerometer data comparison reveal good agreement in the pulse amplitudes with pulse durations of just around 100 s each time the acceleration occurs.
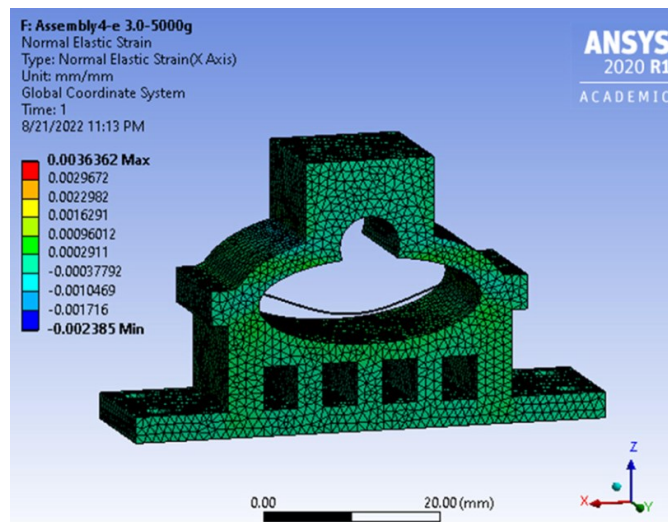
Fig. 5. Finite element method study made in ANSYS [7]

Overall, this study demonstrates the potential of using 3D printing technology to fabricate FBG based acceleration sensors with excellent performance characteristics, which can be customized to meet specific application requirements.

In the study [8] presented in International Journal of Advanced Manufacturing Technology the design and manufacturing of 3D printed robot gripper finger is presented, the design is shown in Fig. 6. The ability to build structures with embedded actuators and sensors is a key challenge in the additive manufacturing (AM) field. By fulfilling this need, AM technologies would advance to a new level in the development of assembly-free smart products, resulting in a reduction in human assembly duties and product costs. The primary innovation in this study is the one shot manufacturing of a soft finger made in 3D printing that has two separate sensors inserted inside it as well as a shape memory alloy (SMA) actuator.
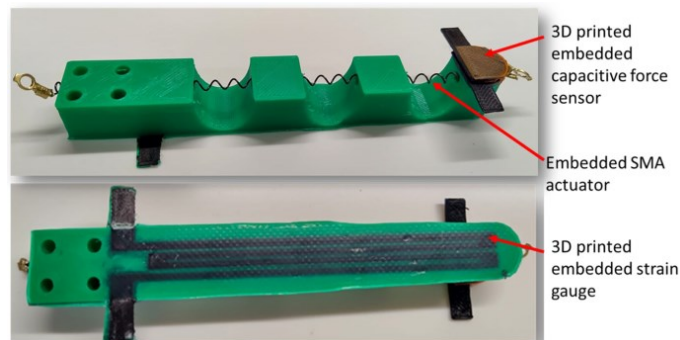
Fig. 6. Manufactured robot finger [8]

The embedded sensor devices allow 3D printed objects created using the suggested method to be instantly activated after being removed from the build plate and to provide real-time feedback. A specially created Cartesian pick and place machine (CPPR) was used to incorporate the SMA spring actuator into the 3D printed robotic finger during the fabrication processes. The inactive components and detecting units of the proposed bioinspired robotic finger were made using three distinct substances from two nozzles. The direct integration of SMA actuators during the 3D printing process is another innovative aspect of the current research. Extrusion of the low melting thermoplastic polycaprolactone (PCL) prevented the activation of the SMA during production since its printing temperature of 70 °C is lower than the austenitic start temperature for SMA. The two integrated 3D

printed sensors allow the suggested finger to be immediately activated after being removed from the 3D printer, delivering real-time input for further needs.
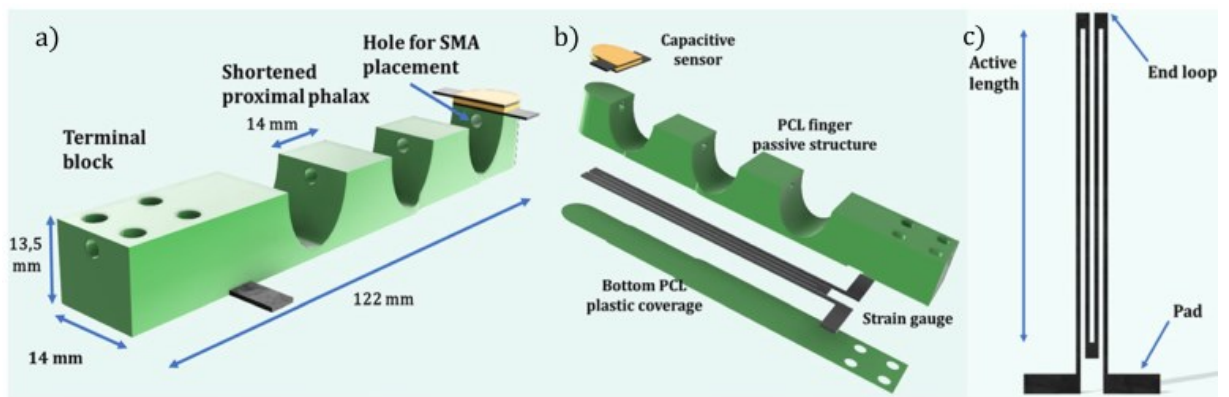
Fig. 7. Strain sensor position in the robotic finger [8]

The sensors were manufactured using a conductive thermoplastic polyurethane (CTPU) called NinjaTek seen in Fig.7., which was chosen to address severe bending that would break conductive polylactic acid (CPLA). However, one of the challenges related to the fabrication of resistive sensors through Fused Filament Fabrication (FFF) is the high electrical resistance (low conductivity) due to the polymeric matrix being doped with conductive fillers like carbon black or carbon nanotubes. Discovering a connection between the FFF procedure parameters and the rise in conductivity is crucial for lowering electrical resistance. According to some study, the final electricity resistance in 3D manufactured strain gauges can be affected by layer height and manufacturing orientation. Two more process variables were looked at in this case study to see how they affected the end result electrical resistance of the a three-dimensional manufactured prototypes.

In the research conducted by scientists from the Toronto university [9], the Fiber Braggs Grating (FBG) [10] sensors, were implemented in the structure using additive manufacturing methods. Tensile fatigue testing of both regular Acrylonitrile Butadiene Styrene (ABS) specimens and ABS specimens with FBG sensors was used to accomplish this. The sample production steps shown in Fig 8. As seen from the picture, first step was to make half of the sample with the grove for the further installation of the optical fiber cable. Afterwards the cable was installed and glued in place, the production process is resumed and the upper layer of the structure is produced. Samples after printing process is seen in Fig.9.
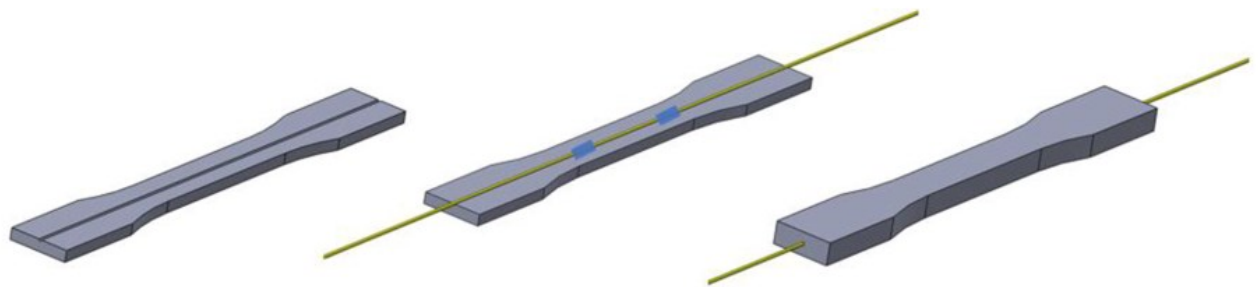
Fig. 8. Three steps of FBG embedding procedure [7]

Optical fibers called Fiber Bragg Gratings (FBGs) are created specifically to reflect particular light wavelengths. They are made via "interference lithography," a method that normally results in periodic

changes in the refractive index of the fiber throughout its length. A portion of the light that enters an FBG is reflected back in the direction it arrived due to the periodic fluctuation in the refractive index acting as a diffraction grating. The distance between the periodic fluctuations in the refractive index, which may be accurately regulated during the manufacturing process, determines the wavelength of light that is reflected.
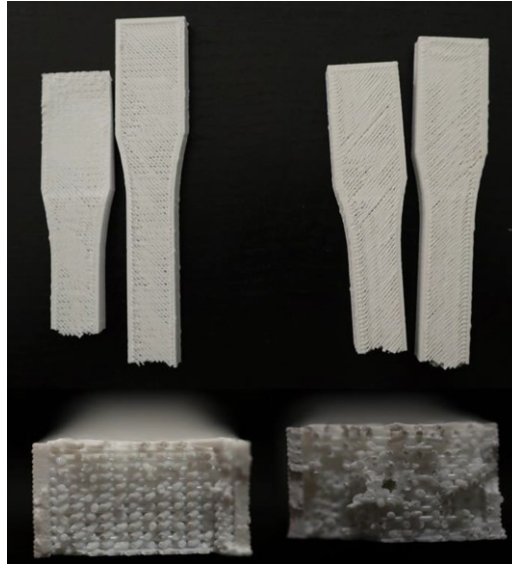
Fig. 9. Samples produced and tested [7]

Due to their ability to detect vibration, temperature, strain, and impact, these sensors are applicable in various fields such as structural, medical, and chemical applications. They are highly sensitive, possess good long term stability, are immune to magnetic and electromagnetic interferences, have a small form factor, are lightweight, and are resistant to corrosion, which contributes to their superior performance [11].

Samples designed to enclose an FBG were 3D printed using the same parameters, with the inclusion of a 0.1 mm hole spanning the length of the sample. The FBG was integrated either by embedding it during the printing process or by inserting it into the sample after printing. They figured out that the filament encompassing the aperture functions as a stiffening bar, enhancing the strength of the sample. This reinforcement is attributable to the fact that the region surrounding the FBG aperture is the only vertically deposited filament layer in the entire sample, and it is deposited in a denser pattern than the remainder of the specimen. The findings indicated that the introduction of the sensor influenced the fatigue life of the specimens to varying degrees at high and low load levels. The aperture was observed to augment the variability in the number of cycles until failure by 80-160% in three of the four load levels. The FBG strain measurements indicated that, despite the reusability of the insertion method, the findings produced were unstable and over 50 times lower than those of finite element simulation. The embedded FBG specimens exhibited a strain response 20-150 times greater than the inserted FBGs, implying that they were more effectively incorporated into the host material. The measurements from the FBG sensors corresponded to the results of finite element simulation of the test specimens subjected to tensile loading.

In the research paper provided by Boise State University in United States, scientist were investigating the additively manufactured sensor idea for tracking state of components of nuclear reactors [12]. The need to monitor strain in challenging environmental conditions is a widespread demand for sensors in various fields. In the context of nuclear reactors, there is a particular interest in strain sensors for

measuring the deformation and vibrations of fuel elements and structural components during reactor power cycles. They were using aerosol jet printing to produce an interdigitated electrode which is a type of electrode configuration used in sensors, actuators, and other devices. It consists of multiple pairs of metallic fingers that are interleaved with each other, forming a comb like pattern. The fingers are typically made of conductive materials such as gold, platinum, or aluminium and can be fabricated on a substrate using microfabrication techniques. IDE are widely used in electrochemical and biosensing applications due to their high sensitivity, low noise, and ability to detect small changes in analyte concentration. The interdigitated design provides a large surface area for interactions with the analyte, resulting in a highly sensitive detection platform [13].

Fig. 10. Thin film Gold Inter Digitated Electrode produced by Micrux Technologies [13]

The design of the interdigitated electrode which is demonstrated in Fig. 11 allows for a low profile capacitance based strain gauge (CSG) with several in-plane electrodes parallel to the substrate, which has demonstrated high strain sensitivity and low hysteresis.
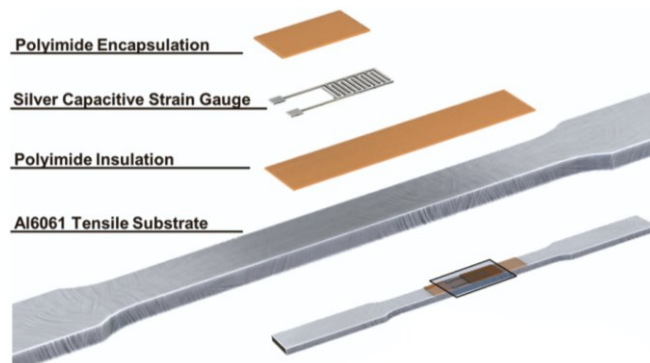
Fig. 11. Schematic of strain sensor application on the sample [12]

The fabrication of interdigitated electrode capacitance based strain gauge involved the use of an aerosol jet printing technique and silver nanoparticle ink, applied onto an ASTM E21 compliant aluminium tensile specimen, as far as aluminium together with stainless steel and zirconium alloys are used in nuclear reactors as cladding material. The printed sensor on substrate shown in Fig.12. Before printing, the surface of the aluminium tensile specimen was cleaned by grinding to remove surface oxidations, followed by a degreasing rinse with acetone and a final rinse with deionized water. Then, a 25 µm thick high temperature polyimide tape, backed with a pressure sensitive silicone-based adhesive, was manually attached to the gauge length of the specimen. To ensure a uniform and consistent starting surface energy for the printed interface, the surface of the polyimide tape was

treated with O2 plasma for 1 minute at 100 watts. While preparing for the research, it was discovered that ceramics are capable of providing effective electrical insulation and stability at high temperatures, but they do not facilitate efficient transfer of strain from the substrate to the top surface where the sensor is located. This results in a phenomenon known as strain shielding and it occurs when a region of a material is shielded from experiencing its full potential strain due to the presence of a stiffer neighbouring region. This happens because the stiffer neighbouring region carries most of the applied load, resulting in a reduction of the strain in the shielded region.
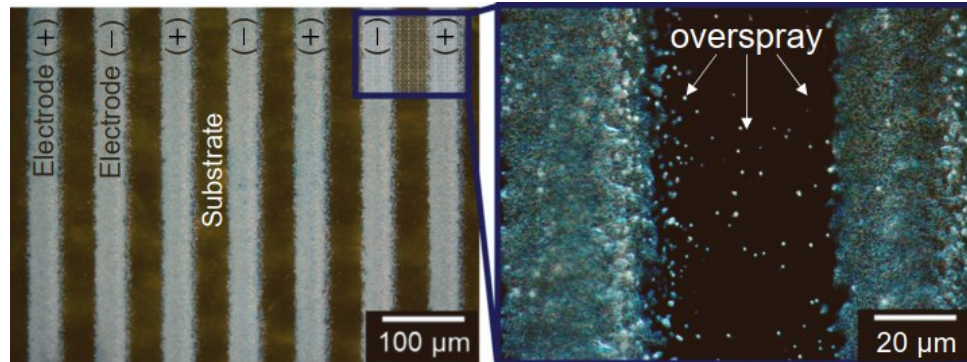
Fig. 12. Stray particles between the electrodes from the aerosol jet printing process [12]

In other words, strain shielding occurs when the load applied to a structure is predominantly carried by a stiff component, leaving a less stiff component to experience less strain than it would if the load was evenly distributed across the entire structure. This can lead to localized failure or deformation in the less stiff component if it is not designed to handle the strain it experiences [14].

The CSG showed high reproducibility and predictability of strain sensing performance; these two factors are important when deploying the strain gauges in field conditions and costly, time consuming experiments. However there were found that they are more sensitive to temperature as compared to the commercially available [12].

This paper by Chinese researchers presents an investigation into the impact of packaging on fiber Bragg gratings. Scientists propose a packaging technology based on 3D printing and verify its feasibility through experimentation. The study examines the effects of the packaging scheme and structure on the sensing characteristics of the FBG, particularly with regards to temperature. The researchers also experimentally analysed the sensing properties and stability of the 3D printed packaged FBG. Results indicate that the FBG can be properly safeguarded and its outstanding stability is guaranteed by its three-dimensional printed packaging development. [15]. Schematic diagram of production shown in Fig. 13.
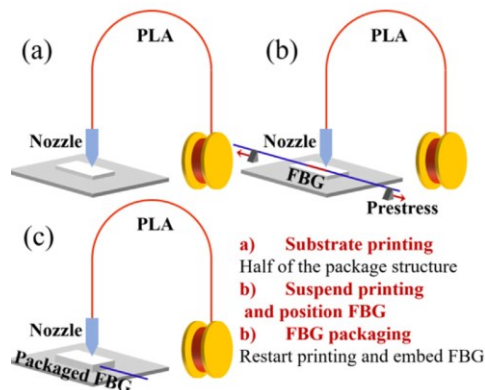
Fig. 13. Schematic diagram of 3D printing-based FBG package [15]

To examine the strain characteristics of the FBG packaged using 3D printing, the strain response is investigated through experimental methods. To carry out the measurements, the packaged FBG is mounted on a 60 mm long cantilever beam fixed onto a platform. The unloaded portion of the cantilever frame is then exposed to displacement using a displacement platform, which alters the strain being applied to the enclosed FBG. Since the displacement is directly proportional to the strain, it is used as a representation of the strain evolution. When the strain applied to the cantilever beam is transferred to the FBG, the packaging structure's geometry changes, leading to a variation in the grating period. This, in turn, causes a shift in the central wavelength, which can be measured to calculate the strain in the FBG. Produced and assembled sensor is displayed in Fig. 14.
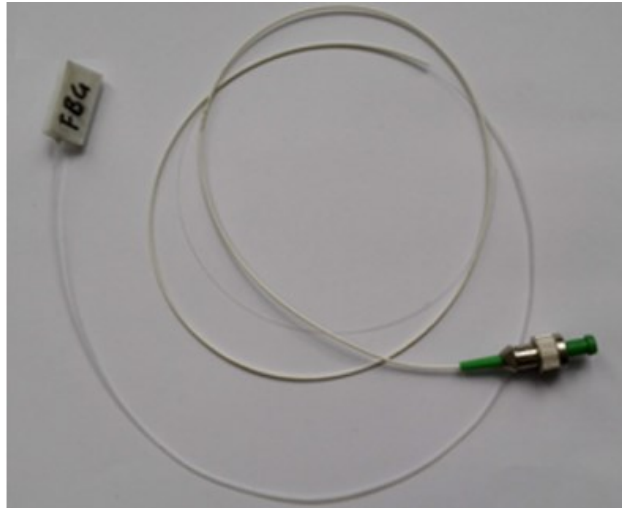
Fig. 14. Produced sensor [15]

The temperature response of the FBG packaged using 3D printing showed variability within different temperature ranges. Gradual decrease in reflection is observed as temperature increases, especially beyond 54 °C. This phenomenon is linked to the thermal deformation of PLA, and the experimental results are consistent with the thermal deformation temperature of PLA, which is approximately 55 °C. Since stability is a critical performance factor, the stability of the 3D printing packaged FBG was investigated, and the results demonstrated that the central wavelength fluctuation is less than 6 pm over a 1 hour period. The measurement error caused by the central wavelength fluctuation is lower than 0,01425 mm and 0,3 °C for displacement and temperature measurement, respectively. The experimental results confirm that this packaging scheme can effectively ensure FBG stability, provided that the sensing characteristics of FBG are maintained.

1.1. Overview Summary

In summary it can be stated the in the industry and also in the researches field there a numerous of innovative concepts and new directions for the proof of concept studies running. Several directions of the researches are seen, including the FPGA technology when the wire is embedded in the 3D printed structure during the printing and provides the data even during the printing process. Based on the 3D knowhow and data, the new type of the sensors, so called, the 4D printed sensors are developed and analysed. This will give additional functionalities and adjustments for the sensors based on environmental conditions, e.g. the temperature, humidity, etc. Having this in mind, the self-adjustable sensors can be produced, and the need of compensation mechanisms can be eliminated in the system, reducing the cost.

2. Methodology

In order to select the right material for the application or the structure the several mechanical properties must be revised. Physical features are required to comprehend and assess the actions of materials, especially plastics, under applied pressures or loads. The following are some of the explanations as to why technical characteristics are important:

Plastic strength is defined as its capacity to endure applied forces without distortion or failure. Tensile endurance, compressive force, and flexural toughness are all included.

Elasticity - a plastic's ability to revert to its initial form after being deformed by an applied force. It is quantified by metrics like modulus of elasticity and Young's modulus.

Hardness - plastic's resistance to permanent denting or scratching. The Rockwell or Shore hardness scales are commonly used to measure it.
Toughness - plastic's capacity to absorb power before fracture. It denotes the resistance of the material to impact or abrupt loads.

Ductility: how much a plastic can undergo stretched or prolonged before splitting. Ductile polymers may be deformed extensively without shattering.

Brittleness: A plastic's tendency to fracture without important deformation when pressured. Brittle polymers breakdown with barely any deformation of the material.

Plastic's capacity to withstand progressive distortion under steady stress over time – creep resistance. It is critical for materials that will be subjected to prolonged stress.

Fatigue resistance - plastic's resistance to breaking down under periodic or recurring stress. Fatigue characteristics are essential for materials that are subjected to dynamic or variable stresses.

Friction and wear resistance - plastic's capacity to endure moving or brushing with another layer without damage or wear.

The mechanical properties of plastics exhibit significant variations depending on the specific type of plastic, its chemical composition, and the inclusion of reinforcing additives or elements that can influence electrical resistance. Based on this information in conclusion, it is important to have strain measurements which are critical in plastics for evaluating flexibility, yield behaviour, ductility, failure analysis, process optimization, and material characterisation. They give vital insights on the mechanical characteristics of plastics, allowing make educated choice of materials, design, and processing decisions to assure longevity, reliability, and safety in a variety of applications.
Hence, a thorough comprehension and establishment of strain measurement principles in 3D printed structures are crucial prerequisites for conducting the study. Moreover, when opting to utilize strain gauges as the primary data source, comprehending the operational principles of strain and establishing the measurement data system and logging device become imperative. With these parameters defined, the manufacturing process can be formulated leveraging 3D printing technologies.

2.1. Definition of the Strain

Strain in materials refers to the deformation or change in shape or size of a material due to the application of an external force or stress. Strain is calculated by measuring the change in length or dimension of a material divided by its original length or dimension [16]. This ratio is typically represented as a decimal or percentage and is expressed as:

$$\varepsilon = \frac{\Delta L}{L},$$ (1)

where: ε is the strain value, dimensionless or expressed in mm/mm, in some cases it can be expressed in macrostrain $\mu\varepsilon$, which is $\varepsilon \times 10^{-6}$. Overall length L in mm and ΔL change in length mm. Visual representation of the strain in shown in Fig. 15.
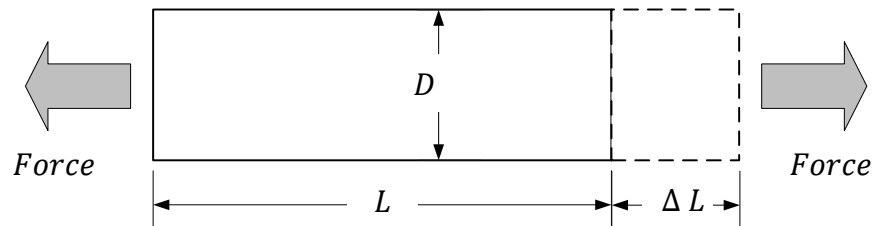
Fig. 15. Definition of the strain

When a uniaxial force is applied to a bar, Poisson Strain occurs, causing the girth of the bar seen in Fig. 15., D, to contract in the transverse direction. The degree of transverse contraction is a material property and is represented by Poisson's Ratio. Poisson's Ratio v is the negative ratio of strain in the transverse direction (perpendicular to the force) to the strain in the axial direction (parallel to the force), expressed as [16]:

$$v = \frac{-\varepsilon_T}{\varepsilon},$$ (2)

Strain is an important parameter in materials science and engineering as it helps to determine a material's mechanical properties and behaviour under different types of loads and stresses. For steel, the Poisson's Ratio ranges from 0,25 to 0,3.

2.2. Strain Gauge measurement

A strain gauge measurement is a technique used to quantify the strain (deformation) of an object or material under applied force or load. It involves attaching a strain gauge, which is a device that changes its electrical resistance in response to applied strain, to the surface of the object. The strain gauge converts the strain into a measurable change in resistance, which can be used to determine the level of deformation. By measuring this change in resistance, the strain gauge measurement can provide information about the strength, durability, and mechanical behaviour of the object or material under stress [17]. The technique is commonly used in various fields, including engineering, materials science, and structural mechanics.

The measurement equipment used in strain gauge measurements typically includes a Wheatstone bridge circuit, it has an electrical stimulation voltage given across the bridge plus four resistance arms. The bridge is connected to a data acquisition system that measures the change in resistance of the strain gauge and provides an output voltage or current proportional to the applied strain. The data

acquisition system can be connected to a computer or other digital device for data processing, analysis, and storage. Additionally, the equipment may include a signal conditioner or amplifier to amplify the low level signal from the Wheatstone bridge and a temperature compensation unit to account for temperature effects on the strain gauge measurements. Other equipment that may be used in conjunction with strain gauge measurements includes load cells, extensometers, and other transducers used to apply force or load to the specimen or structure under test. Strain measurement usually involve quantities smaller than a few milli strain ($\varepsilon \times 10^{-3}$). In order to quantify strain properly, extremely precise changes in resistance must be accurately recorded. With the strain sensors already selected, one step in defining the strain measurement system is to calculate the expected voltage using the provided formula [17]:

$$V_{out} = V_{in} \times \left(\frac{R_x}{R_3 + R_x} - \frac{R_2}{R_1 + R_2} \right), \tag{3}$$

where: V_{in} is the input voltage to the Wheatstone bridge, in volts (V); $R_{1,2,3}$ – resistor values, expressed in ohms (Ω); R_x – strain gauge resistance expressed in ohms (Ω); V_{out}- voltage value after the Wheatstone bridge. Having the assumption that the $R_{1,2,3}$ and the R_x values are the same, the circuit is becoming perfectly balanced, and the output voltage is equal [17]:

$$V_{out} = 0, \tag{4}$$

This situation shows us that the system is working in right way and all values for the resistors are the same. The equilibrium state of the circuit is established by the resistance ratios specified in the following equation [17]:

$$\frac{R_1}{R_3} = \frac{R_2}{R_x}, \tag{5}$$

where $R_{1,2,3}$ – resistor values, expressed in ohms (Ω); R_x – strain gauge resistance expressed in ohms (Ω).

A slight alteration in resistance R_x can render the bridge circuit unbalanced, resulting in a polarity-dependent non zero voltage at V_{out}. Achieving high precision detection of even minute changes requires the use of a differential amplifier to extract the differential signal across the V_{out} terminals and eliminate common mode noise. In a similar manner, to determine the value of R_x based on the output voltage V_{out}, the use of Kirchhoff's Current Law (KCL) and Voltage Law (KVL) results in to the following equation [17]:

$$R_x = \left(\frac{R_2 \times R_3 + R_3 \times (R_1 + R_2) \times \frac{V_{out}}{V_{in}}}{R_1 - (R_1 + R_2) \times \frac{V_{out}}{V_{in}}} \right), \tag{6}$$

By applying this information, we can easy define the changes in resistance of the strain gauge and calculate the ratio of strain ΔR comparing to the original one:

$$\frac{\Delta R}{R_x} = k \times \varepsilon, \tag{7}$$

where: k – the k-factor of strain gauge, ε – is the strain and R_x – strain gauge resistance.
By applying the know values which were listed in data sheet and also the measured values, we can define the strain of the strain sensor and eventually overall system [18]:

$$\varepsilon = \frac{4}{k} \times \frac{V_{out}}{V_{in}} - \varepsilon_s, \qquad\qquad (8)$$

where: k – the k-factor of strain gauge, ε_s – is the apparent strain. Apparent strain is defined as the alteration in the resistance of the strain gauge that is not attributed to the strain applied to the force element. It occurs due to the combined effect of the thermal coefficient of the strain gauge and the mismatch in the expansion rate between the strain gauge and the specimen being tested [19].

2.3. Definition of Structure Geometrical Parameters

For the purposes of the research, multiple samples were specifically designed and manufactured. The samples were intended for tension testing on a specialized equipment, and additional samples were planned for the application of strain gauges on their surface and incorporation within the structure's core layers. Table 1 provides a comprehensive list of the designated samples along with their specific intended purposes.

Table 1. Specimens planned to produce and test

No.	Specimen name:	Quantity, pcs.	Purpose:
1	First sample.	1	Introduction to the 3D printing equipment
2	Second sample.	1	Crack visual inspection under the microscope
3	Third sample (with dummy insert).	1	Divided in half and section used for visual inspection under the microscope
4	Shape according ISO 527-2:2012.	5	Used for the data gathering in testing machine.
5	Shape according ISO 527-2:2012 (with dummy insert).	5	Used for the data gathering in testing machine.
6	Sixth sample with strain gauge mounted on top.	1	Used for the data acquisition system design and tunning. Strain gauge failed.
7	Sample with embedded strain gauge (green).	1	Used for data gathering during testing phase.
8	Sample with embedded strain gauge (grey).	1	Used for data gathering during testing phase.

In essence there were two shapes for the samples planed: according the ISO 527-2:2012 and the shape in dimensions 150x15x3mm, both of them shown in Fig. 16-17.
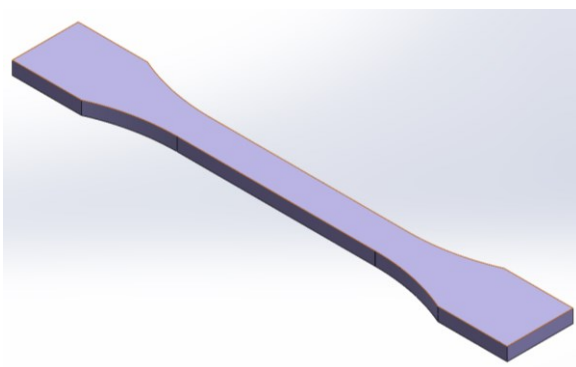
Fig. 16. 3D view of initial specimen design according ISO 527-2:2012 standard.
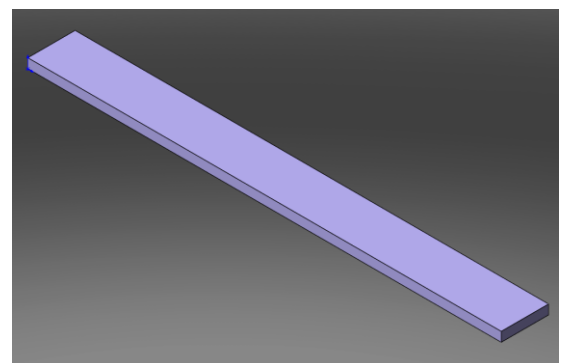
Fig. 17. 3D view of initial specimen design.

The shape and other geometrical properties for the specimens were taken from standard paper and presented in the Table 2 . In the Fig.16. the 3D model of the sample design is shown with the nominal

length of the specimen is 150mm, the width in the widest area is 20mm and in the narrowest part is 10mm. The thickness of the sample is 4mm. The requirements for the shape of the specimen is shown in Fig. 18., and given in mm.
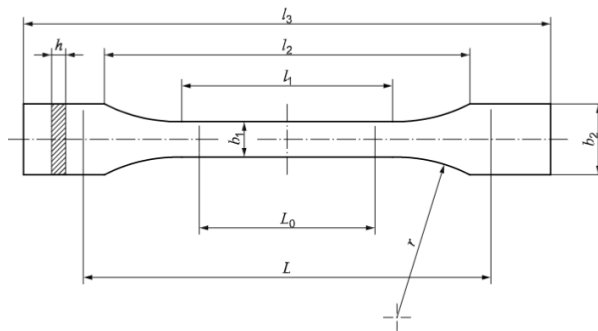
Fig. 18. Geometrical parameters for sample [20]
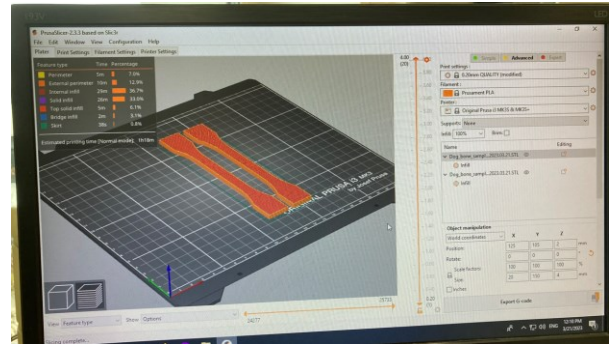
Fig. 19. Prusa Slicer software interface window

Table 2. Dimensions of the specimens according ISO 527-2:2012 [20]

	Specimen type	1B
l_3	Overall length	≥150
l_1	Length on narrow parallel side portion	60,0 ± 0,5
r	Radius	60 ± 0,5
l_2	Distance between broad parallel sided portions	108 ± 1,6
b_2	Width at ends	20,0 ± 0,2
b_1	Width at narrow portion	10,0 ± 0,2
h	Preferred thickness	4,0 ± 0,2
L_0	Gauge length	50,0 ± 0,5
L	Initial distance between grips	115 ± 1

When it comes to the second shape sample the decision was made to use similar dimensions, listed in Table 3., and given in mm.

Table 3. Dimensions of the specimen

	Specimen type	Special shape
L	Overall length	≥150
B	Width at narrow portion	10,0 ± 0,2
H	Preferred thickness	4,0 ± 0,2

For the 3D model data preparation for the 3D printer the Prusa Slicer 2.3.3 software was used to define the parameters for the print and generate the G-code. Interface window is shown in the Fig. 19. In this research, SolidWorks 3D modelling system was the tool of choice for developing the 3D models of the samples. The software's built in tools allowed to create a material library entry with Prusa PLA material properties and calculate the samples weight. The numerical calculated weight is listed in the Table 4. PLA material properties seen appendix No.4. and printer data – appendix.No.6.

Table 4. Sample weight after numerical calculation

Sample name	Weight, grams
1B	10,30
Special shape	8,37

2.4. Definition of Structure Testing Procedure and Equipment

In order to test the samples built and gather data on samples response to load and system excitation the dedicated testing bench is designed and control units defined. The control scheme is shown in the Fig. 20., as it seen from the picture the main components are: signal generator for the load profile signal generation which is amplified in the signal amplifier in order to activate the electromagnet in the test bench. Electromagnet in the test bench is forcing the neodymium magnet mounted on top of the specimen to react and the specimen is loaded according the signal generated. The system response data is monitored and collected using data acquisition system for further analysis.
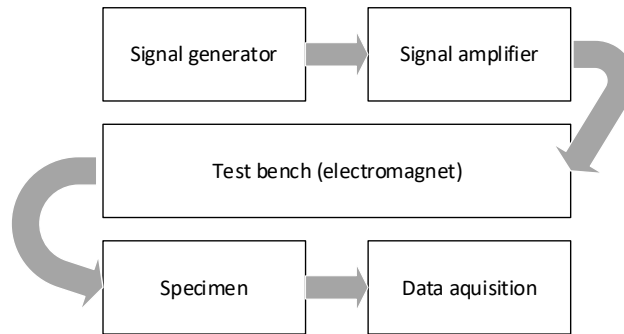
Fig. 20. Control scheme of the test bench control and data acquisition

The schematics of test bench used for the data gathering is shown in Fig.21., the main components are: 1 – bolted connection to the main tapered holder; 2 – the upper U shape profile to fix the specimen in place, 3 - – the lower L shape profile to fix the specimen in place; 4- main pillars to support the specimens holder; 5 – neodymium magnet glued on top with adhesive tape; 6 – specimen; 7- KK-P40/20 electromagnet; 8 – main base plate.
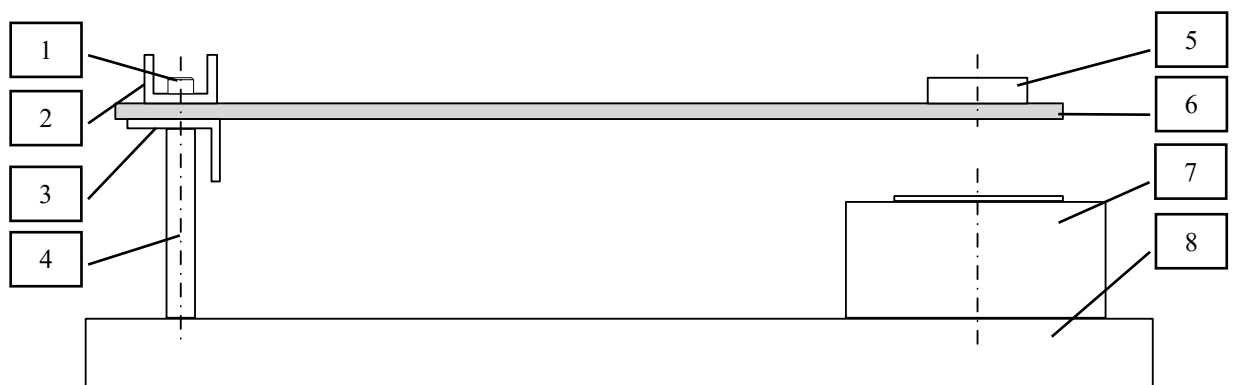
Fig. 21. Scheme of the test bench used for the tests

Distance between the fixture and the electro magnet is approx. 130mm, giving enough space to activate and facilitate neodymium magnet together with the specimen therefore creating the pendulum bending load on the sample.

The following equipment is dedicated to use for the testing bench:
- Rigol DG1032 signal generator, shown in Fig. 22;
- VEB Metra LV102.1 signal amplifier, shown in Fig. 23;

- Mechanical structure acting as main support frame of test bench with integrated KK-P40/20 electromagnet, shown in Fig. 24; and technical data in Appendix No.4.
- Data acquisition system based on Arduino Uno R3 board, shown in Fig. 25;

Fig. 22. Rigol DG1032 signal generator

Fig. 23. LV102.1 signal amplifier
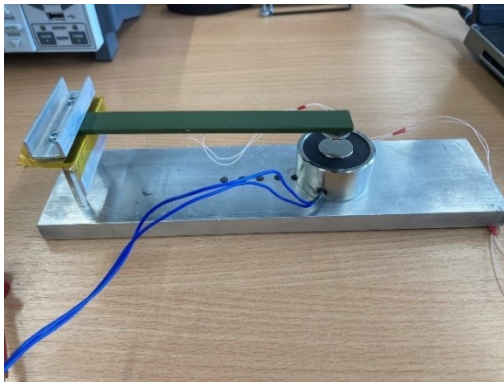
Fig. 24. Test bench assembled
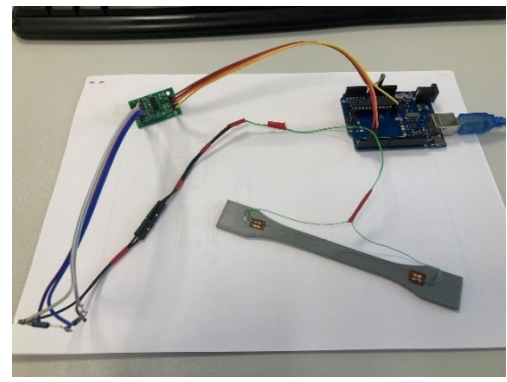
Fig. 25. Data acquisition system

2.5. Impact Test (Bump Test)

To enhance the understanding of the structural behaviour in response to excitation, multiple impact tests were devised, including the bump test. This test involves a deliberate impact, which generates a wide frequency range of structural responses. Its purpose is to analyse the strain sensor response on the structure and gather insights into its characteristics and behaviour under dynamic loading conditions. During the test, the specimen mounted on a test bench, which is designed to replicate the specific type of impact or bump that the product is likely to encounter. The fixture may include features such as drop plates, pendulums, or other devices that can generate impacts with different magnitudes and directions. The purpose of the test is to simulate scenarios in which it may be subjected to mechanical shocks or impacts during use. The test results used to evaluate the structure ability to withstand mechanical shocks and impacts, as well as to identify any design issues. The impact test will be done using the test bench dedicated for the research.

2.6. Testing Equipment Selected

After producing two batches of samples, one of which was left blank without any additional inserts, and the other containing strain gauge imitating dummies made of Kapton tape, all samples were

uniformly prepared for testing using the same equipment. This was done to ensure consistency and accuracy of results. For the material testing the H25KT is a testing machine produced by Tinius Olsen [21], a leading manufacturer of materials testing equipment was used. Machine is shown in Fig.26. This apparatus is made to carry out a variety of tests, such as tensile, compression, flexure, and peel tests, among others. The H25KT features a dual column design for increased stability and precision, and can handle specimens with a maximum load capacity of 25 kN.

Fig. 26. Tinius Olsen H25KT testing machine

The machine is equipped with a digital controller and software, interface is seen in Fig.27, for easy and precise control of test parameters and data acquisition. It also has a variety of safety features, such as emergency stop buttons and overload protection, to ensure safe and reliable operation.
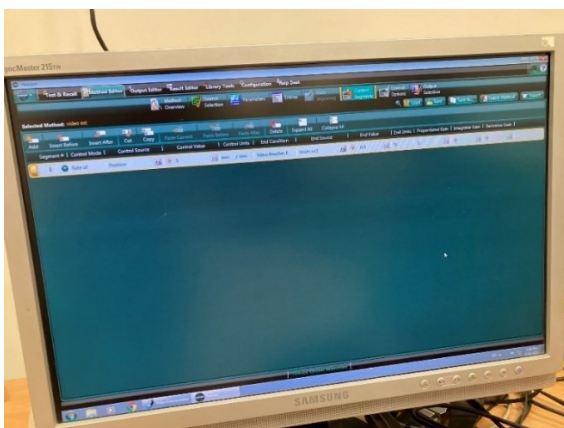
Fig. 27. Tinius Olsen H25KT control interface   **Fig. 28.** VEM 300 series tensiometer [22]

For the extension of the samples in the testing machine, the Tinius Olsen VEM 300 SERIES video extensometer was used. This is a precision testing machine designed to measure the tensile properties of materials. This machine is widely used in materials testing laboratories, research and development facilities, and manufacturing settings to evaluate the mechanical properties of a wide range of materials, including metals, plastics, composites, and textiles [22]. The extensometer is built from

standard technology building blocks, comprising an imaging device and optic, illumination, attachment choices for the machine frame, and data exchange possibilities. Most Tinius Olsen testing equipment structures, such as just one, twin, and four-column machines, are compatible with the VEM 300 series.. The image of the optical extensometer is shown in Fig.28.

2.7. Data Acquisition System Design

In order to gather the data during the tests the data acquisition system (DAQ) is needed. Data acquisition refers to the process of collecting and gathering information or measurements from various sources or sensors. In scientific experiments, data acquisition involves using specialized equipment to collect data related to the experiment's parameters or variables. This data can be in the form of electrical signals, digital values, or other measurable quantities. The collected data is then typically processed, analysed, and interpreted to draw meaningful conclusions and insights about the experiment or phenomenon being studied. The data acquisition process is crucial in ensuring accurate and reliable experimental results [23].

Due the fact that the high precision and speed system with multi-channel data acquisition has limited access, there were decision made to develop the system in frame of research. For this purpose the low cost solution on the Arduino [24] mini-computer base was designed. General view of the system is shown in the Fig.29.

| **Fig. 29.** Arduino Uno R3 board [24] | **Fig. 30.** HX711 load cell amplifier [25] |
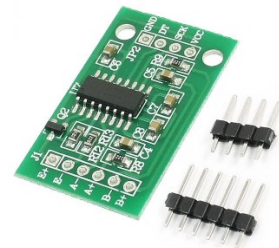
In order to convert the analog signal to digital one and push to the Arduino system for further calculation and processing the one channel load cell amplifier HX711 [25] was selected. Load cell shown in the Fig.30.

In order to have the temperature compensation during the testing phase on the strain gauge, the Wheatstone bridge was used. The Wheatstone bridge is a circuit used to measure an unknown electrical resistance by balancing two legs of a circuit that contain known resistances and a variable resistance. The bridge consists of four resistive legs, with a voltage source applied across one pair of diagonally opposite points and a null detector connected between the other two points. When the variable resistance is adjusted so that no current flows through the null detector, the ratio of the known resistances is equal to the ratio of the unknown resistance to the variable resistance. This allows the unknown resistance to be calculated based on the known resistances and the voltage applied across the circuit. The Wheatstone bridge is commonly used in electrical and electronic measurements, such as in strain gauge measurements, temperature sensing, and in the calibration of instruments [26]. The circuit diagram shown in the Fig.31. Explanation of the components used is made in Table 5.
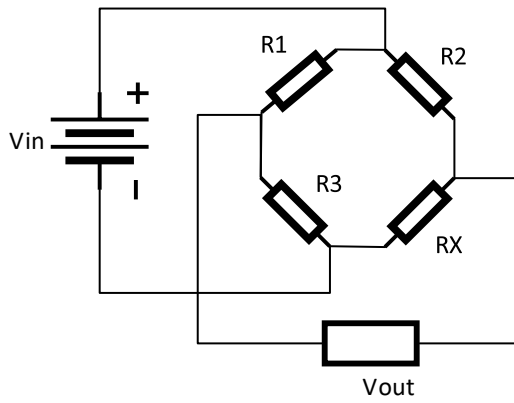
Fig. 31. Wheatstone bridge circuit diagram   **Fig. 32.** Soldering of the Wheatstone bridge
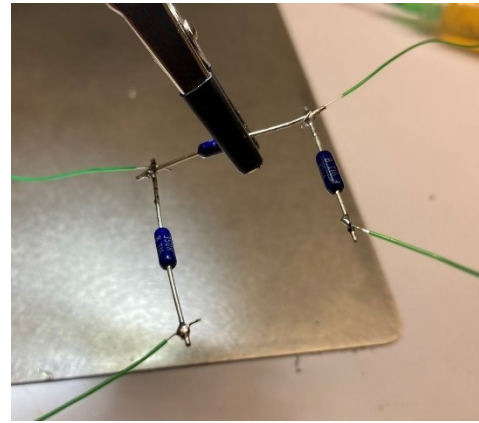
Based on the selected strain gauge resistance, which is 350Ω with a tolerance of ±0.3%, the remaining 3 resistors were selected and obtained. The 350Ω metal film resistors were selected with a tolerance of ±0.1%, produced by Vishay PTF56350, data sheep presented in appendix No.7.

Table 5. Wheatstone bridge components values

Parameter	Value
V_{in}	5 V
V_{out}	0 V (theoretical, when balanced)
R_1	350Ω
R_2	350Ω
R_2	350Ω
R_X (strain gauge)	350Ω

Assembly of the system is seen in the Fig. 33., the resistors were soldered and necessary connections were made by the isolated AWG30 copper wire.

After the preparation of the main components and soldering all parts and wires, the system was connected and tested. The power supply for the amplifier is managed by Arduino board which is connected to the laptop's USB port. Main schematics is shown in the Fig.33. Software code is presented in Appendix No.3.
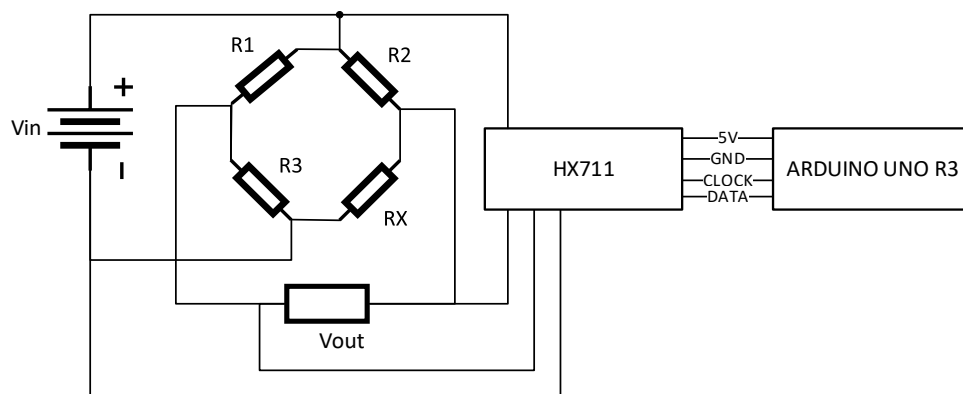
Fig. 33. Data acquisition system design

Assembled system is shown in the Fig. 34. In order to control the measurement data acquisition the control code for the Arduino board was developed and tested. For the development, testing and bug fixing the Arduino IDE version 2.1.0 was used.
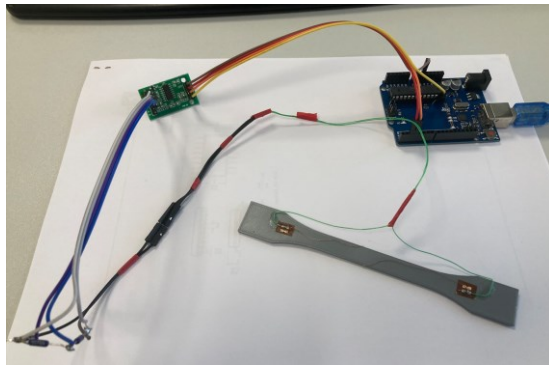
Fig. 34. Assembled system with the sample with embedded gauge
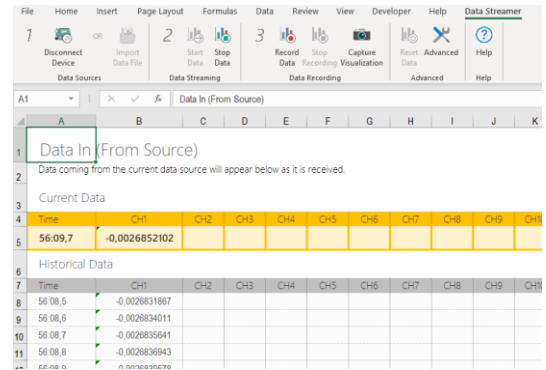
Fig. 35. Microsoft Office Excel Data Streamer Add-on

In order to log all the data obtained during the tests the Excel add in Data Streamer was used, the interface window is shown in the Fig. 35.

2.8. Production of Samples with Embedded Strain Sensor for Further Test

Following the successful integration of strain gauge sensors into the polylactic acid (PLA) structure using a 3D printer and data acquisition system verification, two design samples were subsequently fabricated. In order to have an ability to compare the data obtained, the two different designs were chosen. In the first design, the strain gauge is mounted on top of the structure and in the second one the sensor is embedded in the middle of the structure, near the geometrical centerline.
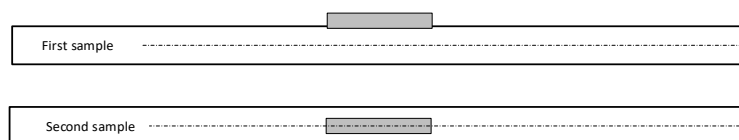
Fig. 36. Schematical section view of structure

The schematics were shown in the Fig.36. where the section view along longitudinal axis is shown and the manufactured samples seen in the Fig.37.

Fig. 37. Manufactured samples with connecting wires

The specimens were subjected to a visual inspection, followed by a verification of their geometric dimensions. Upon confirming their dimensional accuracy, the subsequent steps involved the adhesion

of wire connection plates through the application of an appropriate adhesive and the subsequent soldering of the wiring.

To obtain reliable and accurate data, the strain gauge resistance values were collected using the PeakTech True RMS bench-type multi-meter 4075, which was calibrated prior to the measurements. The measurements were repeated three times, with a three-minute interval between each measurement, to ensure consistency. The resulting averaged data, as shown in Table 9.

Table 6. Resistance measurement results

Name	Resistance, Ω
Sample No.1 (Grey)	350,88
Sample No.2 (Green)	348,87

2.9. Testing of Samples for Young modulus

The Young's modulus, sometimes referred to as the tensile modulus, is a metric for a material's stiffness while it is under tension. It is expressed in units of force per unit area and is defined as the relationship between the tensile stress placed on a material and the strain (usually N/m² or Pa).

The determination of the tensile modulus typically involves a tensile test, which is a common mechanical test used to determine the strength and deformation properties of a material. The test involves applying an axial force to a specimen of a specific geometry and measuring the resulting deformation or strain. The linear section of the stress-strain curve, which represents the region of elastic deformation of the material, has a slope, and this slope is used to compute the tensile modulus [19].

$$E = \frac{\sigma}{\epsilon} = \frac{F/A}{\Delta L /L}, \tag{9}$$

where: E is the Young's modulus (modulus of elasticity); F – force applied (N); σ – stress (Pa); A – cross section area (mm^2); ϵ – strain ; ΔL -change in length (mm); L – initial length (mm).

In order to calculate the Young's modulus we need to have stress:

$$\sigma = \frac{F}{A}, \tag{10}$$

where: σ is the stress value in megapascals (MPa); F is the measured force concerned, expressed in newtons (N); A is the initial cross section area of sample for testing, expressed in square millimetres (mm^2).

Strain calculation

$$\varepsilon = \frac{\Delta L_0}{L_0}, \tag{11}$$

where: ε is the strain value, expressed in dimensionless ratio or percentage; L_0 – is the gauge length of test sample; ΔL_0 is the increase of the test sample in gauge marks expressed in millimetres (mm).

2.10. Summary

In this chapter the methodology for the selection, production and testing of the samples were described and analysed. Mechanical properties of the material analysed and decision made to analyse

the strain of the structure manufactured in the additive technology. For the strain measurement the HBM strain sensor with ability to operate in higher temperatures selected. In order to calculate the influence of the embedded sensor to the structure integrity, the dummy sensors were developed and produced from the polyamide film (Kapton) which is similar to the strain gauge base material, also the dimensions were considered. In order to compare the effect of the embedded train gauge on structure, the five samples with embedded parts and five samples without any additives according the ISO527 standard built and compared in the testing machine. Structures with embedded strain gauges were planed and produced. In order to successfully obtain the data for analysis, the data acquisition system with logging functions planed and implemented.

3. Project Decisions and Results

Several experiments were planned and completed with the aim of collecting additional data and verifying the theoretical assumptions and calculations. The primary objective of this section was to define, design, and manufacture samples utilizing the additive manufacturing equipment that was available. After careful planning and standardization of the sample testing process, it was determined that samples suitable for tensile strength testing in testing machines would be produced. To ensure accuracy and consistency in the testing process, the shape of the samples is defined by the ISO 527-2 [20] standard, which provides guidelines for determining the tensile properties of test samples and specifies the shape that they must take. The ISO 527 standard is an international standard that provides guidelines for determining the tensile properties of plastic materials. It outlines the test methods and procedures that should be used to measure the tensile strength, elongation at break, and modulus of elasticity of plastic materials under tensile stress. The standard specifies the shape and dimensions of the test specimens that should be used, as well as the testing equipment and environmental conditions that should be employed. The goal of this standard is to ensure that the testing process is consistent and repeatable, so that the results can be compared and used to evaluate the properties of different plastic materials. By following these standardized procedures, manufacturers and researchers can make informed decisions about the suitability of plastic materials for various applications and ensure that they are meeting the necessary quality standards. By following this standard, the samples were able to be produced in a precise and uniform manner, which helped to minimize any potential variations or discrepancies in the results. Overall, adherence to established standards and procedures is essential for ensuring the validity and reliability of scientific testing and research.

3.1. Testing Samples Design and Production

In mechanical engineering, a sample [27] refers to a small piece or specimen of a material that is used to test its mechanical properties, such as strength, hardness, elasticity, and ductility. These properties are important for understanding how a material will perform under stress, and can be used to evaluate its suitability for various engineering applications. Samples can be obtained by cutting or machining a small piece from a larger material, or by casting or forming a sample in a specific shape. Once a sample has been obtained, it is typically subjected to various mechanical tests, such as tension, compression, bending, or torsion, in order to measure its mechanical behaviour under different types of stress. The results of these tests can provide valuable information about the material's strength and durability, and can be used to optimize the design of structures and components made from that material. In this research the specimens built in additive manufacturing process by adding material layer by layer using Fussed Deposition Modelling process.

The specimens were produced using Prusa PLA (Polylactic acid) filament [28], which is known for its low melting point of around 175 ° Celsius. Data sheet presented in appendix No. 4.This thermoplastic material can be melted and reshaped several times without significant loss of quality. However, it should be noted that PLA is a hard, but brittle material that tends to shatter when it breaks, which is unlike thermoset materials that cannot be re-melted once they have set. Also not capable of withstanding high temperatures, becoming soft and deforming at temperatures above 60 °C. Additionally, it is susceptible to degradation when exposed to UV light and has inferior mechanical strength, tending to break along the layers or into shards upon impact. Furthermore, the adhesion between layers is weaker compared to other materials.
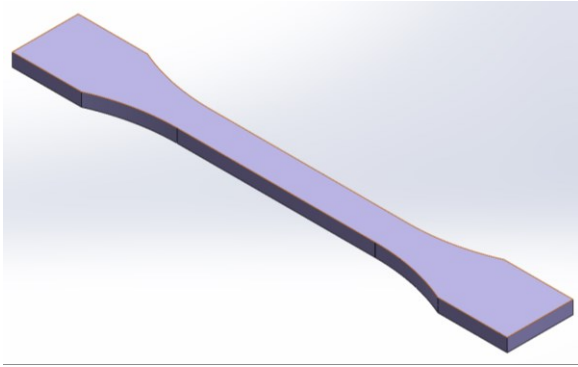
Fig. 38. 3D view of initial specimen design.

Fig. 39. Weighing of the samples.

Table 7. Dimensions of the specimens according ISO 527-2:2012 [20]

	Specimen type	1B
l_3	Overall length	≥150
l_1	Length on narrow parallel side portion	60,0 ± 0,5
r	Radius	60 ± 0,5
l_2	Distance between broad parallel sided portions	108 ± 1,6
b_2	Width at ends	20,0 ± 0,2
b_1	Width at narrow portion	10,0 ± 0,2
h	Preferred thickness	4,0 ± 0,2
L_0	Gauge length	50,0 ± 0,5
L	Initial distance between grips	115 ± 1

For the production of the samples the Original Prusa i3 MK3S+ 3D printer [29] with the production area of 250mm in height, 210mm in 210mm in depth was used.

The weighing of the samples is shown in Table 8. The weighing of the samples was done using the specially obtained precision scales JS13 produced by Bow, with the measurement range 0-500 g and measurement accuracy up to 0.01 g. as seen in Fig. 39.

Table 8. Initial sample batch masses

Sample number	Mass, g.
1	9,86
2	9,84
3	9,86
4	9,90
5	9,89
6	9,92
7	9,93
8	9,94
9	9,93
10	9,94

After the samples design was defined as seen in Fig.38 and calculation were made the batch of 5 pieces were produced according the standard requirements.

The batch of 5 pieces were produced in one time using the same manufacturing machine with same production settings and same material and can be seen in Fig.40. The 3D printer settings shown in the Table 3.
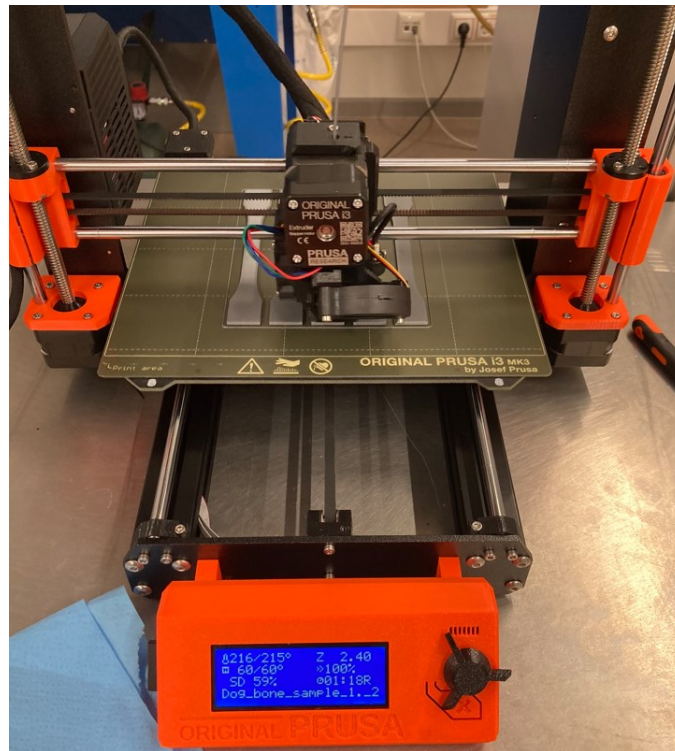
Fig. 40. Original Prusa i3 MK3S+ 3D printer producing samples

Table 9. 3D printer settings

Setting	Value
Nozzle temperature, Cº	215
Print bead temperature, Cº	60
Infill, %.	100
Layer thickness, mm.	0,2
Printing time, min.	192

After the production the visual inspection of the samples it was confirmed that samples are suitable for next stage of testing.

3.2. Strain Gauge Selection

After considering temperature resistibility as the primary selection criteria for the strain measuring sensor, there were explored several types of gauges. Technical parameters, availability, and budget were evaluated before settling on the 1-LM-6/350GE strain gauge produced by HBM for further steps. Data sheet presented in appendix No.1. This specific strain gauge features a foil SG with a measuring grid made of a Cr-Ni special alloy that is 5 μm thick. The carrier is composed of glass fiber reinforced phenolic resin with a thickness of 35 μm, which may deviate by 10 μm. The covering agent is a polyamide foil with a thickness of 65 μm, which may deviate by 15 μm. Copper beryllium tabs with integrated strain relief were used for the connections. The strain resistor has a nominal resistance of 350Ω with a tolerance of ±0.3%. The strain gauge can be used in temperatures up to 250 °Celsius,

which is a crucial property for its application during the 3D printing process. Its gauge factor is around 2.08 ±1.0%. Actual sensors are shown in Fig. 41. Control measurement is seen in Fig. 42.
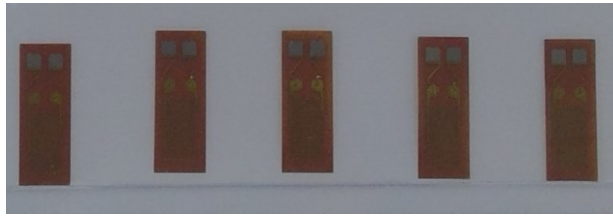
Fig. 41. 1-LM-6/350GE strain gauges
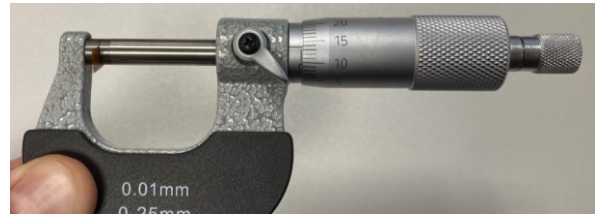
Fig. 42. Thickness measurement of strain gauge

3.3.   Testing Samples with Embedded Sensors Design and Production

As a next step it was planned to build batch of samples with integrated strain gauges and test the influence of the strain gauge on the structure of the testing sample. As far as it was no need for the strain gauges to provide data, it was decision made to embed the mock-up of the strain gauge. As the material for the strain gauge the Kapton tape produced by Pro Power [30] was used, the pictured in the Fig. 43. The tape technical data is shown in Table 4. After the measurement of the strain gauge seen in Fig. 42, the decision was made to use two layers of the Kapton tape in order to have same layer thickness. The main parameter for the Kapton tape is that it withstands temperature up to 280 ° Celsius.

Table 10. Technical data of Kapton tape

No.	Item	Specification	Unit
1	Film Thickness	0,0025 ± 0,002	mm
2	Total Thickness	0,0055 ± 0,004	mm
3	Adhesion	4,6 – 6,4	N
4	Continuous strength	≥ 24	H
5	Tensile Strength	≥ 85	N
6	Heat Resistance	280	Celsius
7	Length	33	m
8	Width	3 – 500	mm
9	Color	Brown	-

For the preparation of the mock-up sensor made of the Kapton tape, the measurement of the strain gauge was made and then the part was cut out of double layer of Kapton tape.

Fig. 43. Kapton tape

Fig. 44. Samples made out of Kapton tape

Samples cut out of the tape displayed in Fig. 44 were used in production of 5 pieces of 3D printed samples.

Table 11. Thickness of Kapton tape layers

Layer	Thickness, µm
1	5,8 - 6
2	11,6 - 12
3	17,5

In order to keep similar thickness to strain gauge, the 2 layers of tape was used. The thickness of the layers combinations is displayed in Table 5.

After the dummies were made and ready for embedding the 3D printing process of the ISO 527 shaped samples out of PLA was started. The printer properties and material properties were used the same as producing the samples without any embedded parts.
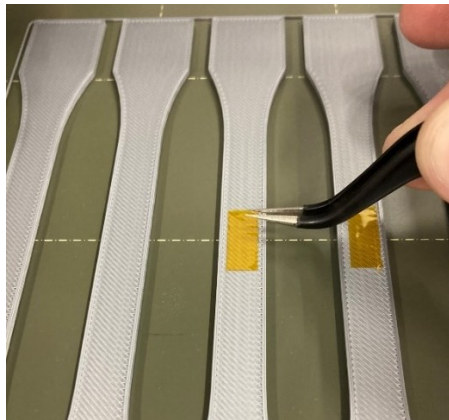
Fig. 45. Application of the embedded sensor dummy
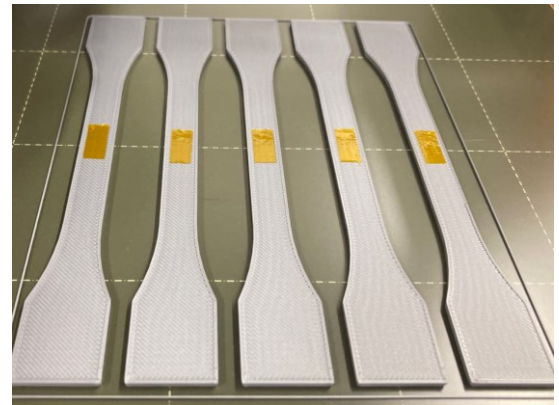
Fig. 46. Samples ready for resume of production

Production process is paused in the middle of the printing process, when the sample thickness reached the 2 mm, and then the Kapton made inserts were applied and sticked on samples as seen in the Fig.45 and in Fig.46. After the application and validation of position the printing process resumed and proceeded to the end of it.
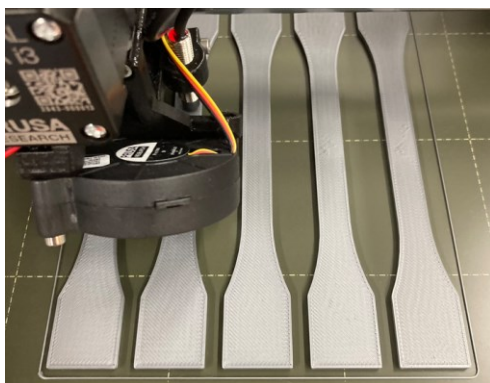
Fig. 47. Production of the samples after the dummies inserted

Fig. 48. Samples right after production

After the production, seen in Fig. 47. the samples underwent a thorough inspection to identify any discrepancies and were marked accordingly for future project requirements as seen in Fig. 48. To keep track of which samples have been tested samples marking is needed to help ensure that there is no test the same sample multiple time and also to indicate important characteristics of the samples. The characteristics marking is seen in Fig. 49.
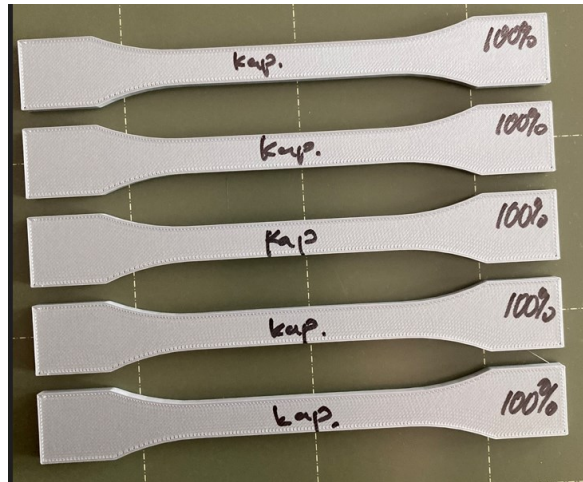
Fig. 49. Samples ready for testing

3.4. Testing of the Samples Produced

Prior to conducting the tests using the universal testing machine, the relevant geometrical information of the samples is collected, recorded, and documented meticulously. For the section area calculation the 3 measuring points were selected for each of samples and data gathered, the averaged data is specified in Table 5. Sampling points were shown in Fig. 50.
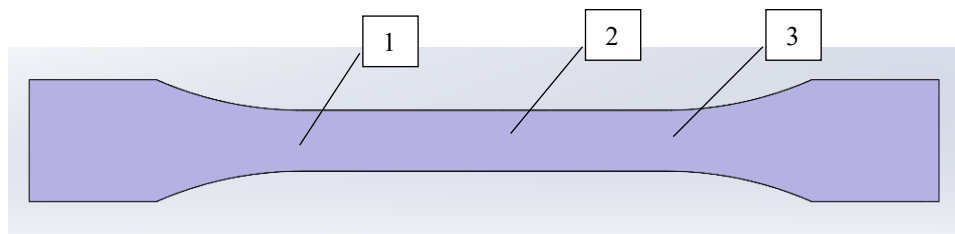
Fig. 50. Positions of measurement data gathering places

Table 12. Geometrical data or the samples

No.	Description	Section width, mm.	Section height, mm.	Section area, mm²
1	-	9,97	4,03	40,16
2	-	9,99	4,02	40,16
3	-	9,97	3,95	39,34
4	-	9,98	3,98	39,72
5	-	10,02	4,01	40,21
6	with apton insert	9,95	4,05	40,28
7	with kapton insert	10,00	4,09	40,92
8	with kapton insert	9,99	4,18	41,74
9	with kapton insert	9,99	4,15	41,47
10	with kapton insert	10,00	4,15	41,53

3.4.1. Testing Samples for Youngs Modulus

In order to compare the samples with dummy insert and without any inserts the following test was made to calculate the Young's modulus. The test machine was set to the stop when the 0,3 % of the strain will be reached. The data show in Table No. 13. represents the modulus calculated. Calculation methodology is described in formulas 9-11.

Table 13. Calculate tensile modulus

No.	Description	Tensile modulus, MPa.	Tensile modulus PLA, MPa.
1	-	2,166	
2	-	2,011	
3	-	1,969	
4	-	2,052	
5	-	2,073	2,2
6	with kapton insert	1,883	
7	with kapton insert	1,895	
8	with kapton insert	1,812	
9	with kapton insert	1,864	
10	with kapton insert	2,057	

3.4.2. Testing Samples till the Breakdown

In order to understand the insert effect on the structure, the samples were tested in the testing machine till the breakage and the force needed was registered, the first 5 samples were tested without any inserts. Results are shown in the Fig.51. As it seen for the data, the force needed to disrupt the sample is approx. 1500 N.
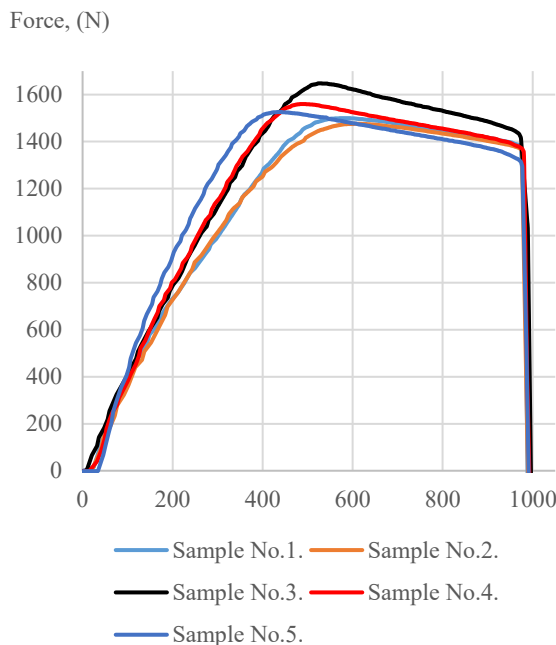
Fig. 51. Samples with no insert   **Fig. 52.** Samples with insert
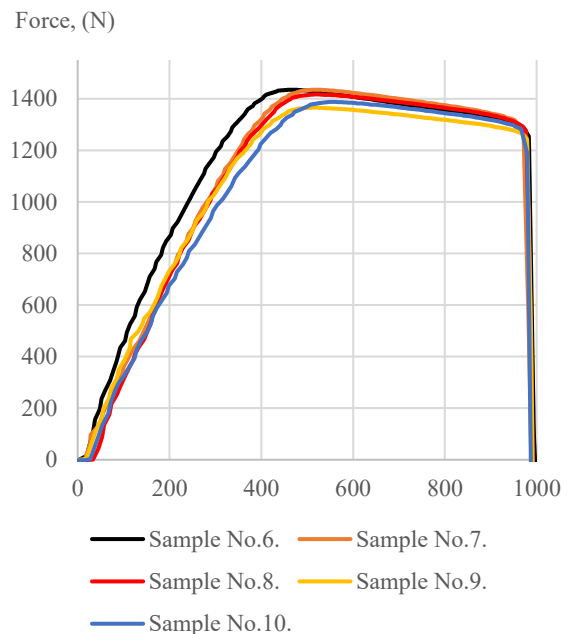
Same test were done with the second sample group in order to register force needed, the data is shown in the Fig.52. The force need is shown in the Table No. 14. The physical damage points are seen in the Fig. 53-54.

Fig. 53 Samples after the disintegration

Fig. 54. Samples with strain gauge dummy after the disintegration

During the test till the samples breakage the samples were destructed, as seen for the photo in Fig. 56, the breakage point in most of the cases is out of the area where the insert is embedded. This gives an idea, that the insert does not affect the sample and crack is formed in the other area. But the applied force is approx. 8% lower in order to reach the point of breakage comparing to the samples without dummy insert. Only on sample No.3., the disintegration was detected in the area of planned strain gauge as seen in Fig.55.

Table 14. Force applied

No.	Description	Force, N.	Average force, N.
1	-	1500	
2	-	1476	
3	-	1648	1542
4	-	1560	
5	-	1526	
6	with kapton insert	1435	
7	with kapton insert	1435	
8	with kapton insert	1417	1408
9	with kapton insert	1366	
10	with kapton insert	1388	

3.5. Visual Inspection of the Samples Produced

Visual inspection is a non-destructive testing technique used to assess the physical characteristics of an object or material through unaided or aided visual observation. This technique can provide important information about the object's condition, including its shape, colour, texture, and surface features. Visual inspection is widely employed in numerous fields, such as engineering, manufacturing, and material science, and can be performed at various stages of production or in-service use. It is a cost-effective and versatile method that can be used to identify surface defects, cracks, corrosion, and other abnormalities that may affect the object's performance or durability. The results of visual inspection can be further enhanced through the use of specialized equipment, such as image magnification glass, microscopes or borescopes, to facilitate a more detailed examination of the object's surface or internal structures [31]. To acquire further insights into the effect of embedded strain gauges on the mechanical behaviour of the structure, it was determined that employing a dummy material acting as a strain gauge was necessary. The Kapton tape was chosen as the ideal dummy material due to its robust mechanical properties and exceptional ability to endure high temperatures of up to 280°Celsius, thus ensuring accurate results. In essence, the selection of Kapton tape as a dummy material provides a reliable means of evaluating the influence of embedded strain gauges on the mechanical properties of the structure. In order to conduct visual inspection the samples were cut apart in the area where the dummy material was implemented. For the visual inspection two devices were used: Nikon Eclipse LV150 microscope with integrated photo capturing device and Delta Optical Discovery L stereo microscope without photo imaging capabilities.
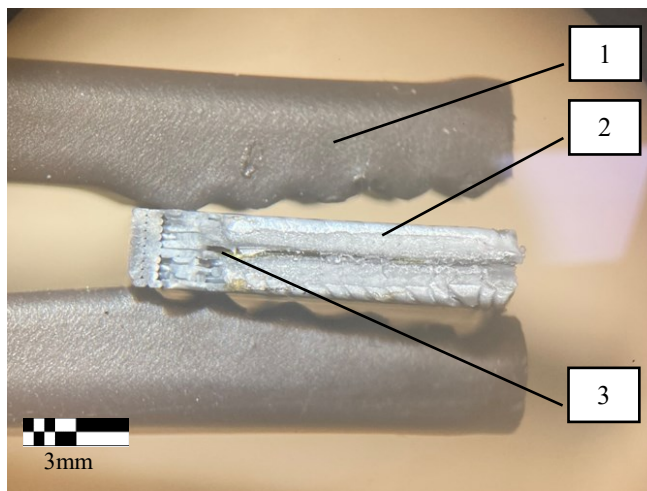
Fig. 55. Sample in the gripper; (1) gripper; (2) structure; (3) embedded material
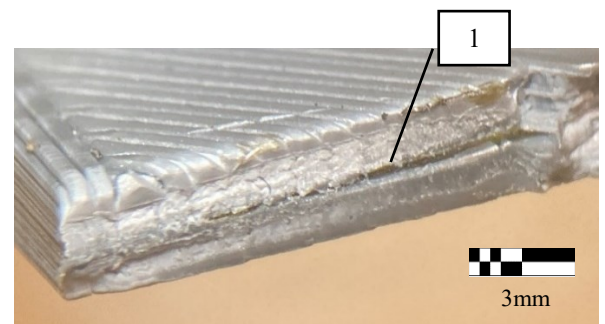
Fig. 56. Divided sample; (1) embedded material

Figures 55-56 depict images obtained through utilization of the Delta Optical Discovery L stereo microscope. These images readily reveal the presence of the embedded material and allow for its clear differentiation even through unaided visual observation. Additionally, it is evident that the production process did not incur any adverse effects on the embedded material, as its initial dimensions and sizes were well-maintained. Notably, the initial phase of inspection did not involve surface grinding following the cutting process, as evidenced by the depicted figures.

In the subsequent stage of visual examination, the Nikon Eclipse LV150 microscope was employed, following the prior preparation of samples by utilizing PS8A P320 sanding paper to grind the section surface, thereby achieving a surface of optimal smoothness.

Fig. 57. Cut through sample; (1) embedded material shown

Fig. 58. Cut through and grinded sample; (1) embedded material shown

Figures 57-69 exhibit the observed characteristics resulting from a visual inspection of a cut-through specimen. Fig. 60. exhibit the PLA layers near the edge of the division, as it can be seen the cut-out have straight ends of the layers.

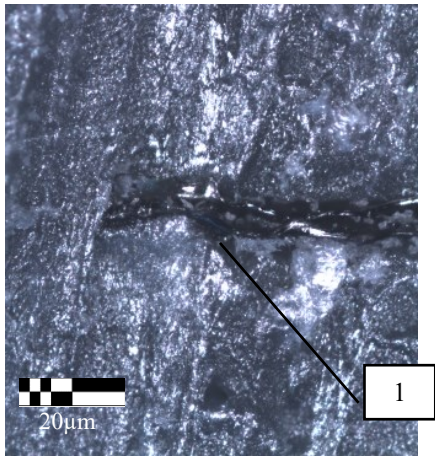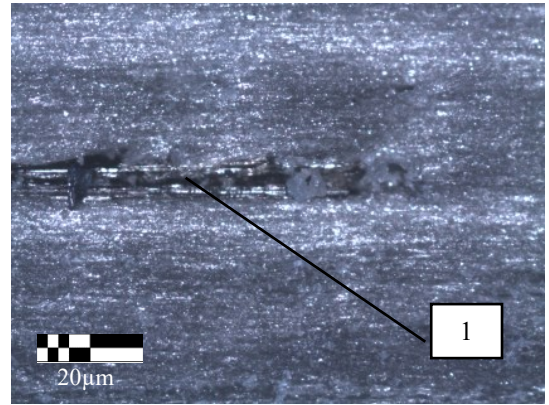Based on the visual evidence provided by the images, it can be concluded that the presence of the embedded material has not compromised the overall structural integrity of the specimen. No discernible gaps, cracks, or other defects are visible.
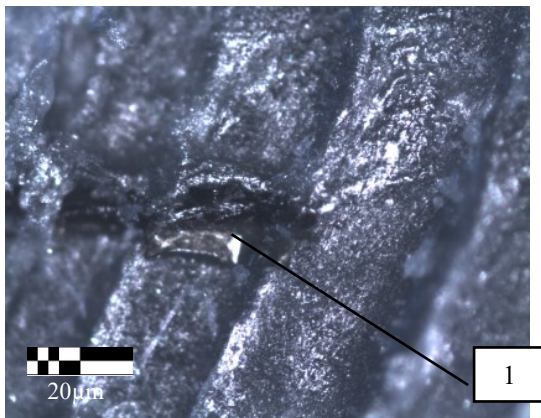
Fig. 59. Cut through sample; (1) embedded material shown
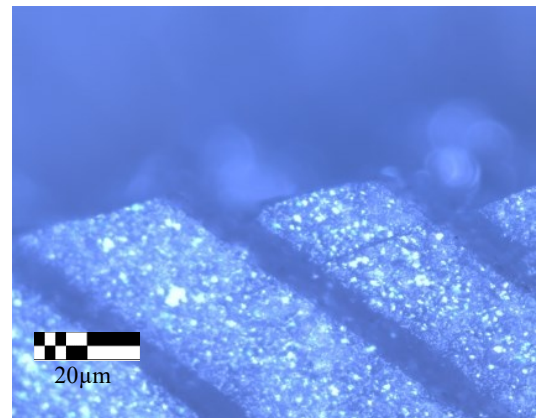
Fig. 60. Cut through sample, top view, the breakage shown.

3.6. Production of Sample with Embedded Strain Sensor

After conducting a thorough analysis of the samples and gathering relevant information, the subsequent step involved producing new samples with embedded strain sensors utilizing the advanced techniques of additive manufacturing. This was undertaken to further enhance the capabilities of the samples by integrating sensors that would provide real-time strain measurement data during testing and operation. By doing so, it was expected that the samples would demonstrate improved performance and reliability in a range of applications.

In order to select a strain measuring sensor that could withstand high temperatures, various types of gauges were examined based on technical parameters, availability, and budget. After evaluation, the 1-LM-6/350GE strain gauge produced by HBM was chosen for further project steps. This particular

strain gauge is composed of a measuring grid made of Cr-Ni special alloy with a thickness of 5 μm and a carrier made of glass fiber reinforced phenolic resin with a thickness of 35 μm (with a possible deviation of 10 μm). The covering agent is a polyamide foil with a thickness of 65 μm (with a possible deviation of 15 μm). Copper beryllium tabs with integrated strain relief were used for the connections. The nominal resistance of the strain resistor is 350Ω with a tolerance of ±0.3%. The strain gauge has an application temperature range of up to 250 ° Celsius, which is its main property for use in 3D printing processes. The gauge factor is approximately 2.08 ±1.0%. Fig. 61 shows the actual sensor (1) with soldered copper wires (2) selected for the project.
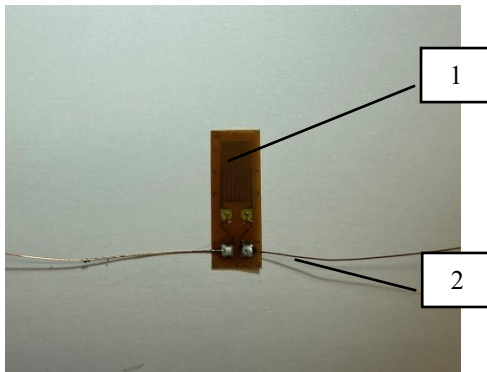
Fig. 61. Stain gauge with coper wires attached.

Fig. 62. 3D printer settings

Following the successful soldering of wires to the strain gauge, the resistance measurement was carried out to verify the functionality of the system. Once this was confirmed, the 3D printing equipment was prepared for the subsequent production of the sample. The settings for the Prusa printer were adjusted as depicted in Figure 62, with the nozzle temperature set at 215 ° Celsius, and the working pad temperature set at 60 ° Celsius.

These optimized settings were chosen to ensure the accurate and precise production of the sample using the 3D printing technology. Following the necessary calibration steps, the 3D printer was prepared. The production data was then loaded and the production process was initiated. The progression of the production process was visually monitored and recorded in Fig. 63.
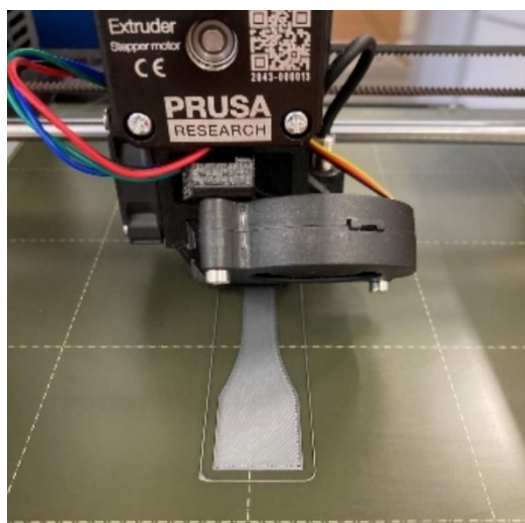
Fig. 63. Production in progress
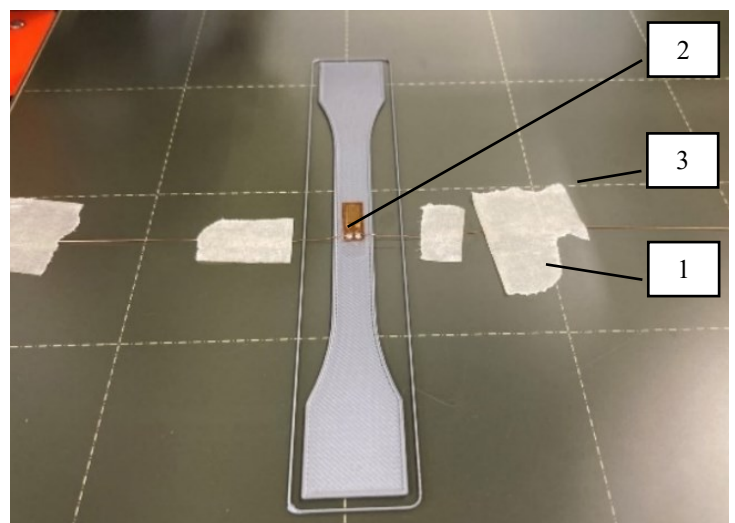
Fig. 64. Stain gauge glued on the PLA structure.

In the midst of the process, the production was temporarily halted to attach a pre-prepared strain gauge with soldered wires to the middle of the sample, as demonstrated in Fig. 64. This facilitated the placement of the measurement (2) grid in the central region of the construction. The wires were temporarily secured to the printing bed (3) with paper tape (1). After allowing sufficient time for the fast curing glue Z70 produced by company HBM, to cure and ensuring the firm attachment of the strain gauge, the printing process was resumed, and additional final layers of the material were printed on top to complete the construction.

Subsequently, the functionality of the strain gauge was evaluated by measuring its resistance level. This measurement was conducted by interconnecting the sensor wires (1) with the measurement device wires using gripers as illustrated in Fig.65. Upon completion of the connection process, the resistance of the strain gauge was measured using the PeakTech True Rms bench type multi-meter 4075 and confirmed that it is in the rage of stated by manufacturer in Fig.66. By doing this it was confirmed that the strain gauge is in healthy state and it can be used for further steps in research project.
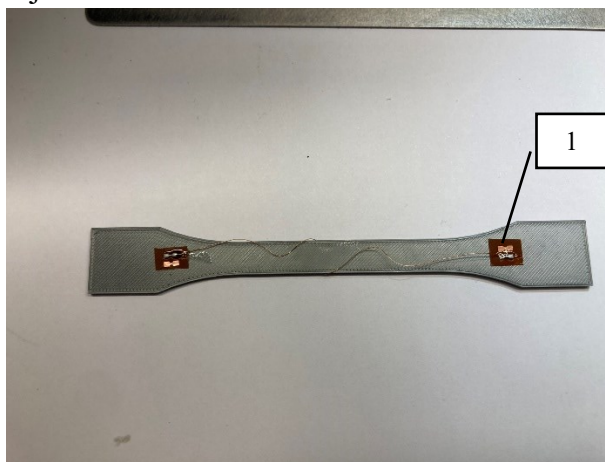
Fig. 65. Sample built with embedded strain gauge

Fig. 66. Measuring resistance of strain gauge

Once the sample has been produced and its resistance value measured in a static mode, the subsequent step involves monitoring the strain gauge data changes during the blending of the sample. This would provide crucial insights into how the sample responds to different conditions.

To validate the accuracy of the strain gauge, a set of preliminary tests were conducted, involving the slight deformation of the sample's shape and the subsequent tracking of resistance changes. The gauge's functionality was verified by carefully considering any observed changes. This crucial step enabled the progression of further actions towards the completion of the experiment.

Upon successful integration of the strain gauge into the 3D printed structure and subsequent confirmation of sensor health, further steps can be taken in the research and the additional samples for calculation can be produced.

3.7. Experiment and Data Collection

Following the confirmation of the trustworthiness of the data acquisition system and the preparation of samples, a test plan was devised and executed. As the first the testing equipment was selected and testing rig was built. The first step involved the selection of testing equipment and the construction of a testing rig.

The initial phase of the experiment involved testing specimens that were affixed with strain gauge on their upper surface. The primary objective was to investigate the response of these specimen to loading and changes in load profiles. The resulting data, depicted in Fig. 67, illustrates the voltage response and reaction of the specimen No.1 (Grey) to increasing forces as it is bent in both directions. As seen from the illustration some retention is seen also.
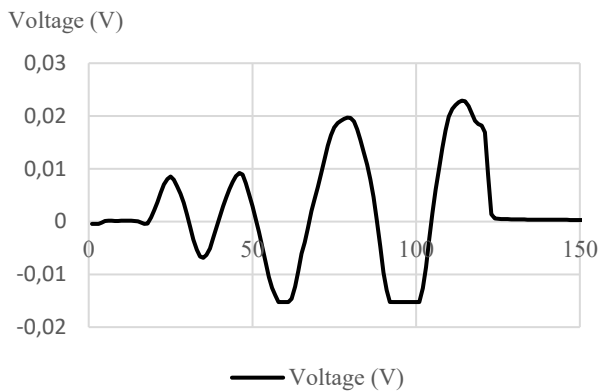
Fig. 67. Voltage change under the load change
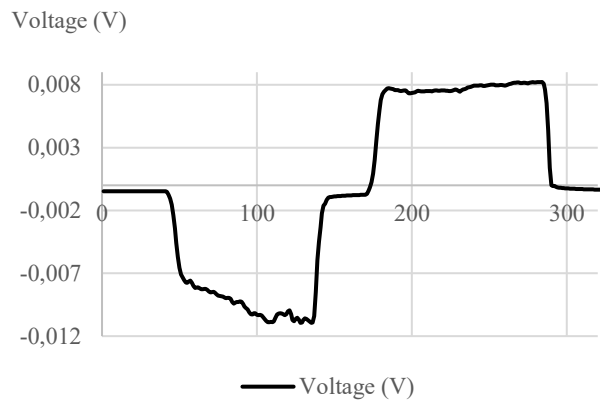
Fig. 68. Voltage change under the load change

Fig. 68 displays the voltage fluctuation observed during an experiment performed on specimen No. 1 (grey). The experiment involved subjecting the specimen to unidirectional bending, followed by a pause, release, and subsequent bending in the opposite direction, again followed by a pause and release, all performed under controlled conditions.

In Fig. 69, the voltage fluctuation recorded during an experiment on specimen No.1 (grey) is presented. The experiment involved subjecting the specimen to unidirectional bending, with no pause between each direction change. As a result, a smooth transition is observed from one peak to the opposite peak. However the excitation of the system is not controlled.
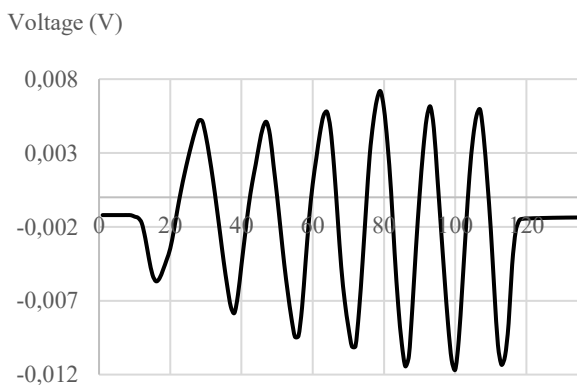
Fig. 69. Voltage change under the load change
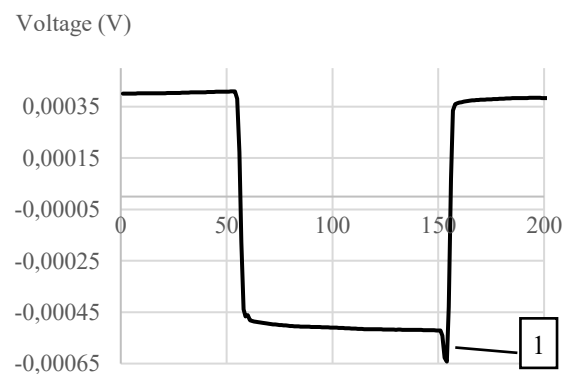
Fig. 70. Voltage due the fixed load application

Fig. 70 depicts the voltage variation resulting from the application of a fixed 50 grams weight load on the end of the specimen. The graph illustrates that the loading and unloading of the weight were detected, including a minor overload (l), caused by the manual placement of the weight.

It also can be see that then the load was applied the system stabilized only before the unloading, this can be improved by extending the test time.
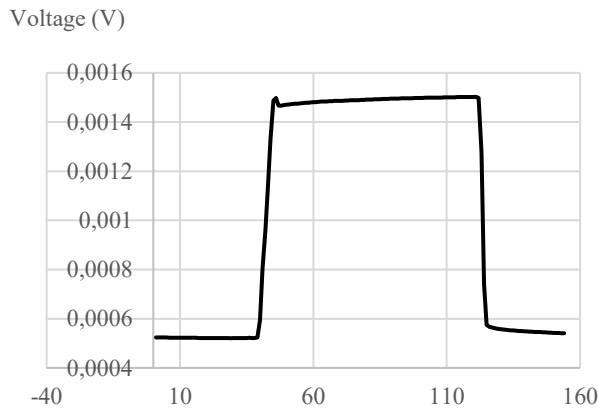
Fig. 71. Voltage change due the inverted fixed load application
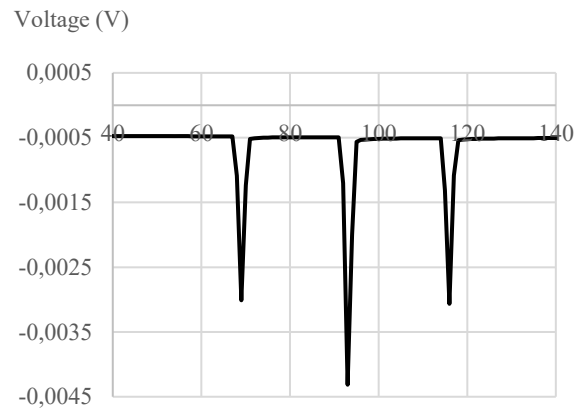
Fig. 72. Voltage change due the three non-controlled bumps applied.

In Fig. 71, the variation resulting from the application of a fixed 50-gram weight load on the end of the specimen is displayed. However, the specimen was inverted in such a way that the strain gauge was positioned at the bottom. As it can be seen from Fig.70-71 the data obtained is inverted. Fig. 72 depicts the response of a structure to three randomly applied bumps, with the resulting data indicating an immediate change in the response.

The structure was tested on a testing bench using different excitation frequencies, with three tests performed at frequencies of 1Hz, 2Hz, and 3Hz. The results, shown in Fig. 73, indicate that the stability of the signal is acceptable, despite some shifting, which may be attributed to various factors, including system stability. Fig. 74 illustrates the system response when a load is applied to the end of a specimen that is fixed and bent at the beam's end. The response obtained is good, although the signal stability is not optimal.
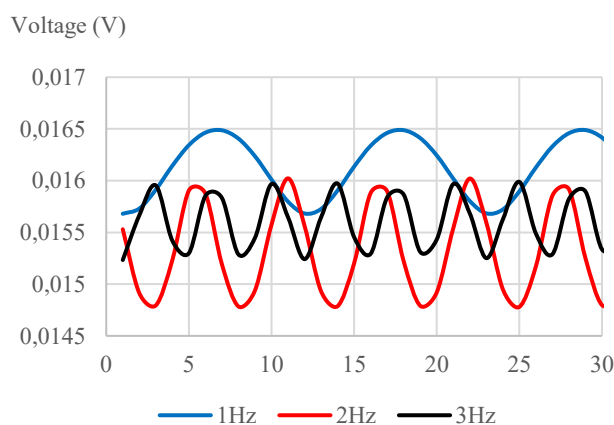
Fig. 73. Comparison between different frequencies
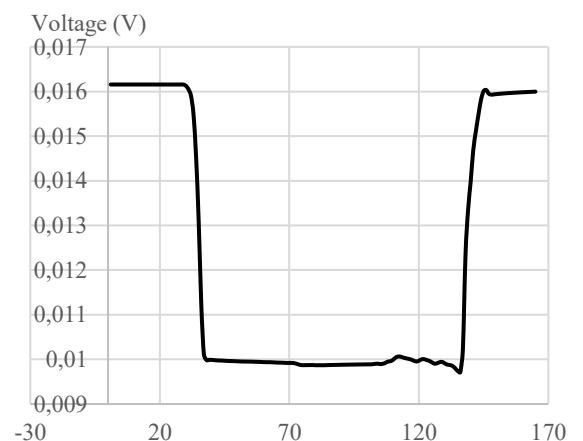
Fig. 74. Voltage drop due load change

After the tests performed with the specimen No. 1 (Grey), the next step was to proceed with specimen No. 2 (Green) and perform the same tests. In the Fig. 75, the changes in the system responses is seen due the application of bending force on the end of the beam and fixing it for some time, similar pattern

50

is seen on Fig. 76., where the load is fixed 50 gram loaded on the end of the beam and left for some time, after that the load is removed.
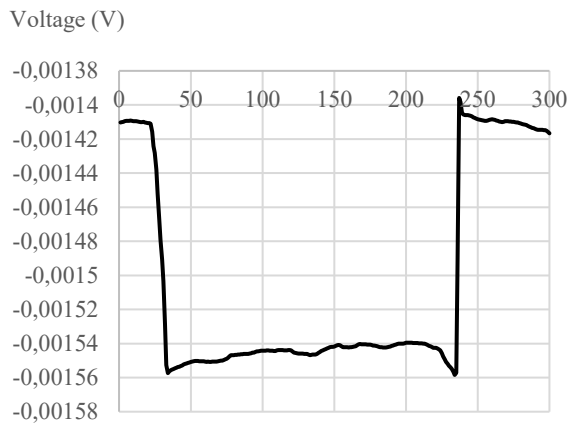
Fig. 75 Voltage drop due fixed load
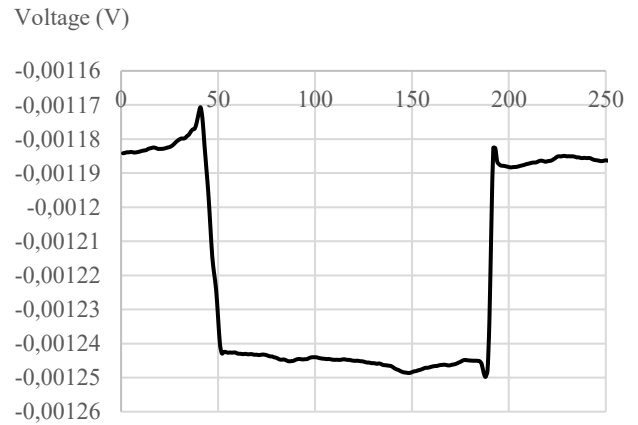
Fig. 76. Voltage change due 50 gram load

The bump tests were also performed on second specimen, the Fig. 77., demonstrates the system response to the randomly applied bump, with the resulting data indicating an immediate change in the response. The structure was also tested on a testing bench using different excitation frequencies, with two tests performed at frequencies of 1Hz and 3Hz. The results, shown in Figure 78, indicate that the stability of the signal is acceptable, also it is observed, that the shifting is not that extreme in this case.
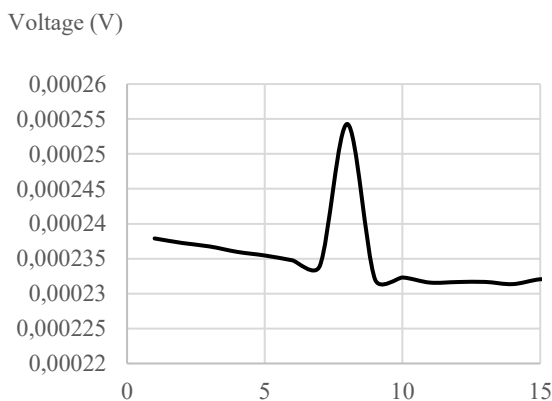

Fig. 77. Voltage change due the non-controlled bump applied.
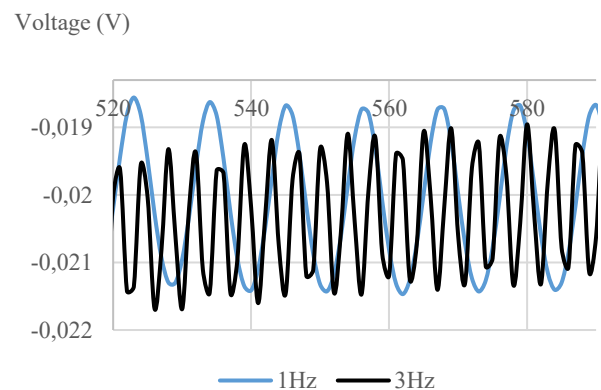
Fig. 78 Comparison between different frequencies

The data presented in the figures show the response of two specimens, No. 1 and No. 2, to various loading conditions. The tests involved applying a fixed weight load to the specimens and subjecting them to bending forces, with the resulting data indicating changes in the system response under these conditions. The stability of the signal varied, with some shifting observed due to factors such as system stability, etc. However, overall, the response obtained from the specimens was considered good, although the signal stability could be improved. These findings provide valuable insights into the behaviour and characteristics of the materials being tested, which could potentially inform the development of new materials with improved mechanical properties and contribute to the design and engineering of structures subjected to similar loading conditions. In the Fig. 79-80. the testing bench with the specimens is shown.
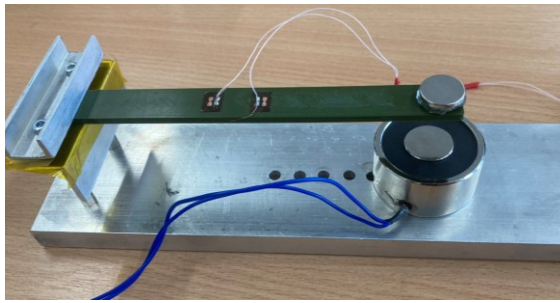
Fig. 79. Sample, No.2, under testing
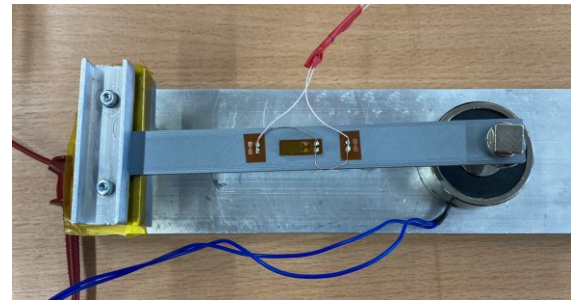
Fig. 80. Sample, No.1, under testing

3.8. Samples Testing for Strain Measurement Data Validation

In order to gain more data and know how about the specimens with integrated strain gauges the tests in the testing machine were conducted. The testing machine Tinius Olsen H25KT with VEM 300 series tensiometer was used. The first test conducted, was tension of the specimen No. 1. (Grey) up to 0,3% of length, with the speed of 2mm per minute.
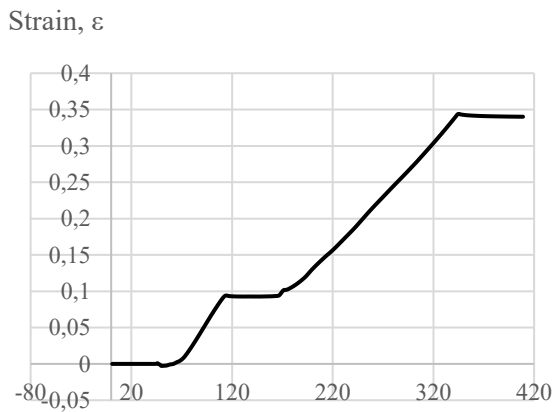
Fig. 81. Strain measured on sample No.1. (1st)
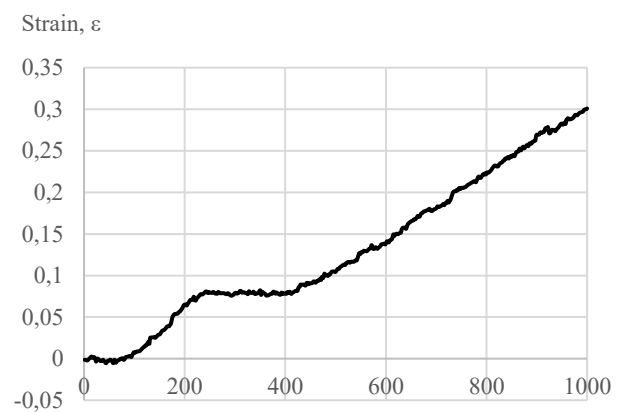
Fig. 82. Strain measured via extensometer (1st)
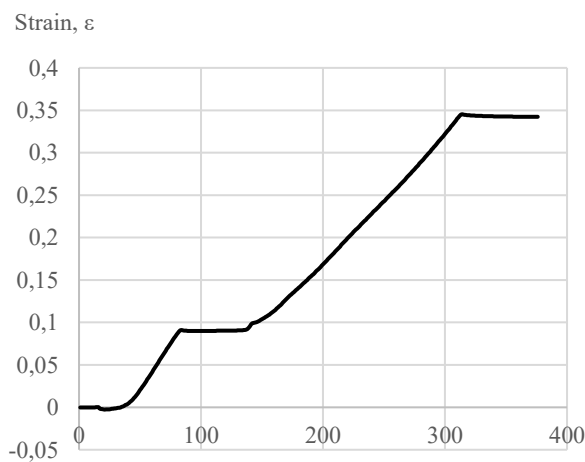
Fig. 83. Strain measured on sample No.1. (2nd)
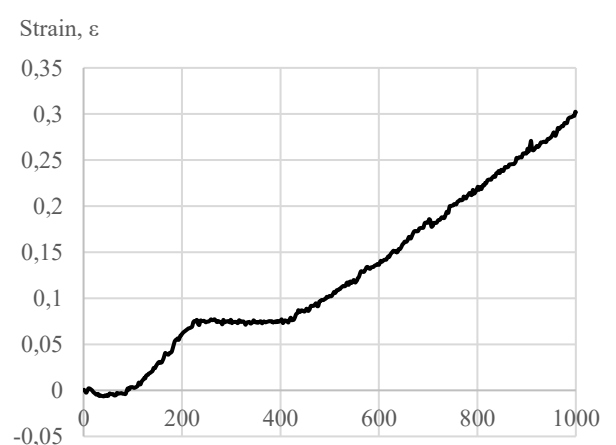
Fig. 84. Strain measured via extensometer (2nd)

In total there were three test runs conducted using the same specimen and the same testing conditions and the data gathering with DAQ based on Arduino microcontroller. The obtained dada from the

embedded strain sensor is shown in the Fig. 81,83 and 85, the data delivered by extensimeter is shown in the Fig. 82,84 and 86. As it can be judged from data comparison, the strain data is similar and it can be detected discrepancies on the testing machine e.g. Fig.83-84.
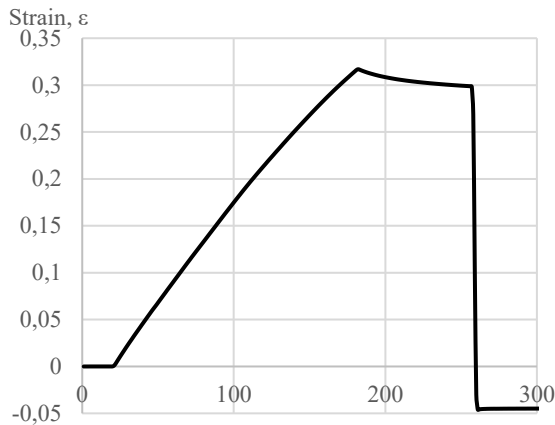
Fig. 85. Strain measured on sample No.1. (3rd)
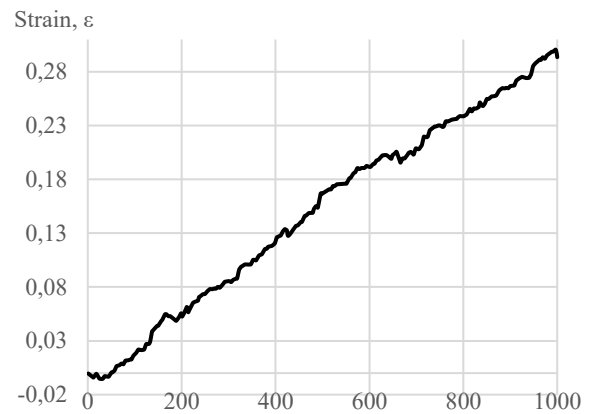
Fig. 86. Strain measured via extensometer (3rd)

During the final, 3rd run on the same conditions, the strain detected by the strain gauge Fig.85 and the strain measured by the equipment Fig.86 is nearly the same, giving us a good indication that strain gauge is detecting strain in optimal way, the difference of the measurement is shown in Table No.13.
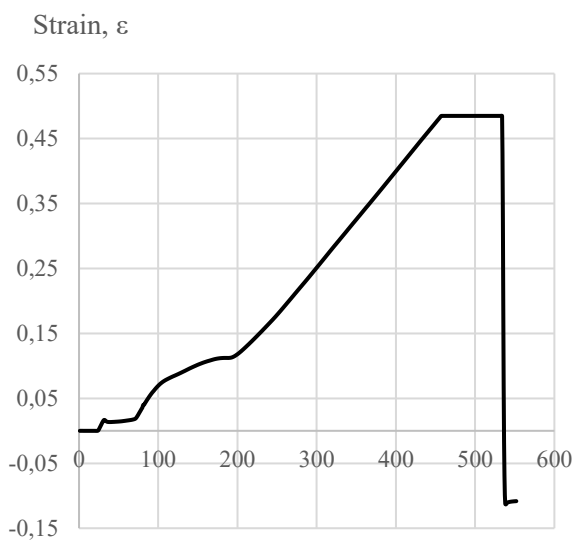
Fig. 87. Strain measured on sample No.1. (4th)
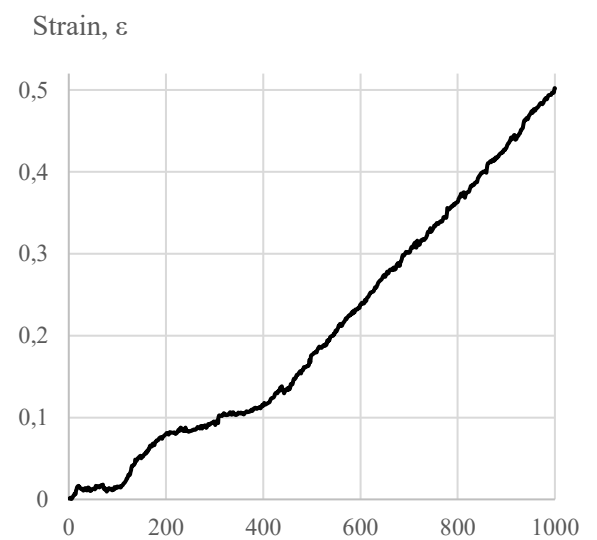
Fig. 88. Strain measured via extensometer (4th)

For the same specimen is t was planned to have a test run No.4. on following conditions: strain up to 0,5% of length, with the speed of 5mm per minute, the data shown in the Fig.87-88. As it seen for the data comparison in the Table No. 15, the maximal detected strain via strain gauge and detected via extensometer is similar and differs only about 0,017, which is optimal result.

The second test conducted was tension of the specimen No. 2. (Green) up to 0,3% of length, with the speed of 2mm per minute. The strain detected via the embedded strain sensor is shown on the Fig. 89 and Fig. 91, the data for the extensometer is seen in the Fig.90 and Fig.92.
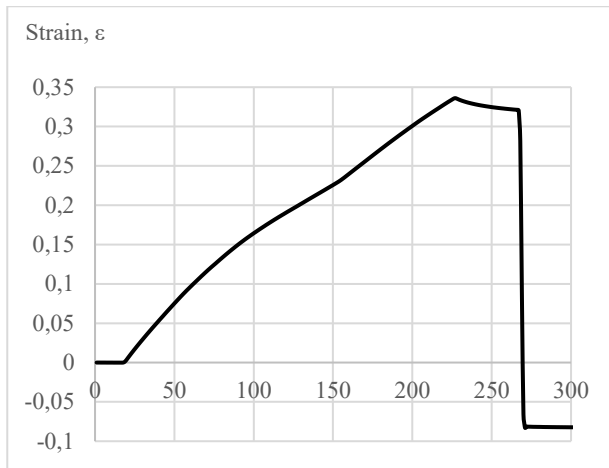
Fig. 89. Strain measured on sample No.2. (1st)
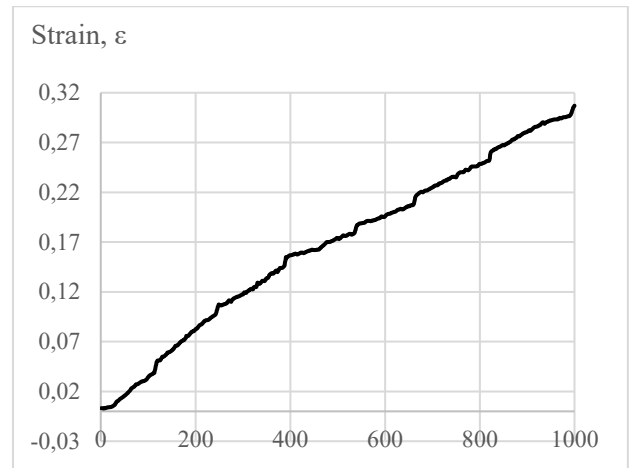
Fig. 90. Strain measured via extensometer (1st)

From the strain measurement obtained during the test of the specimen No. 2. (Green), it can be stated the that the 3D printed structure with integrated strain gauge corresponds to the load conditions change in fast and acceptable time and detects the strain change in accurate way. This serves as a proof of concept and confirms that embedding of strain gauge gives advantage.
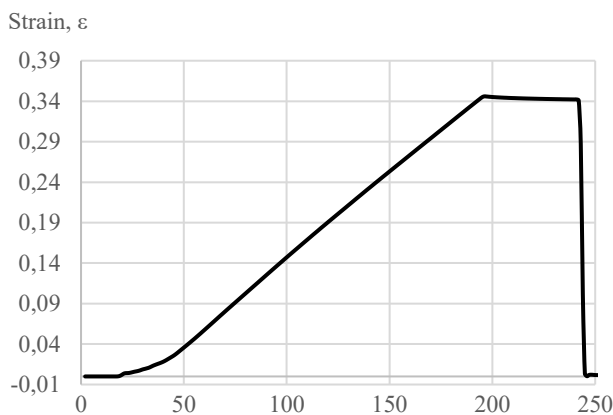
Fig. 91. Strain measured on sample No.2. (2nd)
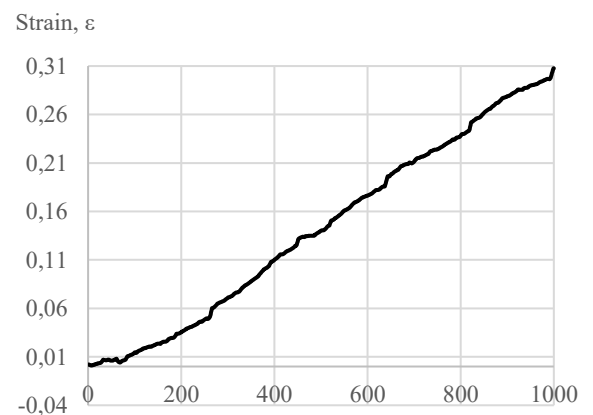
Fig. 92. Strain measured via extensometer (2nd)

Table 15. Maximal value of the strain detected

| Test run, No. | Specimen | Maximum strain detected, ε | | Strain difference |
		Embedded strain gauge	Optical extensometer	
1.	No.1. Grey	0,343987	0,300900	0,043087
2.	No.1. Grey	0,345349	0,302400	0,042949
3.	No.1. Grey	0,316916	0,300500	0,016416
4.	No.1. Grey	0,484891	0,502200	0,017310
1.	No.2. Green	0,336094	0,307000	0,029094
2.	No.2. Green	0,345956	0,307700	0,038256

The data obtained shows us that the both samples are active and the data can be obtained and recorded. As seen from the Fig.83., the specimen responds to the loading profile created by the test machine which is shown in Fig.84, without the pause and unloading. Based on this data it can be stated that

specimen with strain gauge on the top surface and with embedded strain gauge can be used for further research.

3.9. Summary of Tests

In summary it can be stated the that result of samples production and testing was implemented successfully, in order to gain more knowledge about the structure, several visual inspection loops were made. Important part of the research was to produce the samples with integrated dummy parts acting as a sensor and afterwards integrate the sensors itself during production. Based on data gained it can be sated that the result is positive and strain gauges can be embedded in various 3D printed structures. Also it is important to mention that the data acquisition part takes significant part in the overall test phase and it must be prepared in best way. In overall it can be stated that the testing phase is successful.

4. Cost and Benefit Analysis

Cost benefit analysis is a method used in mechanical engineering to assess the feasibility and profitability of a project or investment. It involves comparing the total costs of a project or investment with its expected benefits, in order to determine whether it is financially viable and worthwhile. In mechanical engineering, the costs may include expenses related to materials, labour, equipment, maintenance, and other relevant factors. The benefits may include increased efficiency, reduced downtime, improved safety, higher production output, and other desirable outcomes.

4.1. Strain Gauge Sensor Application and Installation Costs

Main component for the embed strain measurement is the strain gauge, which is embedded in the 3D printed structure. Strain sensor was selected keeping in mind the elevated temperature impact during the printing process, therefore the price range is higher also. The strain sensor used for the embedding has price of 189,00 € for the package of 10 pieces, keeping that in mind we got the cost of 18,90 € / pcs. Comparing to the standard range of the strain gauges e.g. 1-LY41-3-700, which cost around the 102,00 € per 10 pcs., giving us cost of 10,20 € / pcs. This shows us that the special strain sensor dedicated for the elevated temperatures increase the costs approx. by 54 %. Both strain gauges were produced by the company HBM and have similar precision class.

When it comes to the installation of the strain gauge on the structure, the special type of glue, 1-Z70 by HBM, were used in order to attach strain gauge on the surface, the package consist of 10ml glue, which is enough for 10 pcs. The price for the glue are 75,00 € / bottle. This gives us approx. 7,50 € per one strain gauge installation. Moreover the soldering pads 1-LS5 also should be considered with the price of 80,00 € / 125 pairs, datasheet for it presented in appendix No.2. For one strain gauge one pair it is needed and it gives us 0,64 € of cost. It total the costs excluding the labour cost and soldering material it is 37,24 €. These cost were generated in any case, because there is a need to attach the strain sensor to the specimen no matter will it be mounted on top of it or it will be embedded.

4.2. Data Acquisition System Costs

To obtain a comprehensive understanding of data acquisition systems, several company products were evaluated to gather information regarding their associated costs.

Fig. 93. 1-MX440B QuantumX Universal Amplifier [32]

Fig. 94. 4-Channel Compact DAQ Voltage Measurement Bundle [33]

Table 16. Costs comparison for various DAQ systems

Name	Cost, €.
1-MX440B QuantumX	5120 [32]
4-Channel CompactDAQ	1250 [33]

In order to conduct a comparative analysis, two 4-channel data acquisition (DAQ) systems were evaluated for their suitability in measuring strain gauge data in a professional context. The first system, the 1-MX440B Quantum X Universal Amplifier, produced by HBM and depicted in Fig. 93, was compared to the second system, the 4-Channel Compact DAQ Voltage Measurement Bundle, produced by National Instruments and shown in Fig. 94. Both systems require a significant initial investment, as outlined in Table 16.

As a cost-effective alternative to professional level DAQ systems, the Arduino Uno R3 development board coupled with the HX711 load cell amplifier can be utilized. The Arduino board, priced at approximately 28,90 € [34], and the amplifier, priced at 3,70 € [35], result in a total cost of 32,60 €, presenting a significant cost reduction. However, it should be noted that the HX711 load cell amplifier can only measure a single strain gauge, while professional-level systems can measure up to 4 channels. Therefore, taking this into account, the total cost for the same number of channels using the Arduino Uno R3 development board and HX711 amplifier could increase up to 130,40 €.

However comparing the two 4-channel DAQ systems, which cost over 1000 € each, to a cheaper alternative that costs approx. 150 € may highlight significant differences in performance, features, and data quality. However, the suitability of the cheaper alternative for a professional context would need to be evaluated carefully before considering it as a viable option.

4.3. Labour Costs

Labour costs in new product development from an engineering perspective refer to the expenses related to the creation, testing, and manufacturing of a new product. This involves the time and resources needed by engineers, designers, technicians, and other staff to develop and evaluate prototypes, refine the product design, and prepare for large-scale production. Labour costs may also include expenditures associated with project management, documentation, and quality control. The engineering labour costs represent a significant aspect of the overall budget for new product development and can vary depending on the intricacy of the product, the level of expertise required, and the geographical location of the development team. These expenses are typically closely monitored and managed to ensure the cost-efficient and efficient development of the product. In this case the direct engineering hours dedicated to 3D printed structure design, manufacturing, procurement and software development were presented in Table 17.

Table 17. Working hours required

Description:	Hours, h.:
Engineering	80
Procurement	30
Preparation for manufacturing	40
Manufacturing	8
Assembly	20
Software development	60
Tests on test bench	40
Testing in tension machine	5

In total, the generated amount is approximately 283 direct working hours, equivalent to approximately 7 weeks, considering a 40 hour work week. Based on the salary level in the industry [36] we can resume that the hourly rate is approx. 20,00 €, giving us 5660,00 € total in labour cost for the research.

Based on information provided it can be concluded that the customized solution is beneficial for the market and there are significant cost saving available if the integration the strain sensor is present.

4.4. Cost and Benefit Analysis Summary

Based on data obtained and calculation made it can be stated that alternative and more cost effective solutions can be used for the strain gauge data acquisition systems. Based on the data quality and logging abilities the decision on the DAQ must be made.

Conclusions

1. Methodology for manufacturing of structures with embedded sensors was made and successfully implemented during the development of the samples for tests. As a first stage it was 3 samples built according the shape defined in the ISO 527 standard in order to adjust and tune the 3D manufacturing machine Prusa MK3S. The PLA as material for the structure was selected. After the tuning phase it was defined that the best solution is to use the 100% infill level and 0,2 layer thickness, because in this case the surface is mostly flat and the strain gauge application is optimal. In order to define the effect of the integrated sensor on the mechanical properties of the structure, it was produced batch of 5 samples with no additives working as dummy sensors and batch of 5 specimens with dummy sensors made out of the Kapton tape, which has very good temperature stability up to 280°Celsius and acts in similar way as base material for the strain gauge. The specimen shape taken out of the ISO 527 standard. Moreover there were the visual inspection made on digital microscope Nikon Eclipse LV150 and Delta Optical Discovery L stereo microscope to have the visual inspection of the cut out area of dummy sensor integration which showed that the material adhesion to the Kapton tape is acceptable and there were no discrepancies detected which affect the data from the strain gauge. Visual inspection showed that the sensor, which has thickness of 0,0025mm embeds in good way. After the validation of the strain gauge implementation, the following batch of specimens were produced with the 1-LM-6/350GE strain gauge from the HBM with the ability to withstand the elevated temperatures up to the 250 °Celsius with the strain resistor has a nominal resistance of 350Ω. The live sensor integration was made following the process created during the manufacturing of the samples with dummy inserts. After the successful integration of strain gauges on and in the structures the test phase was released.

2. The impact to the structures was made and several testing phases in testing machine was made in order to get data for analysis. It was detected that for the size of samples used the impact on structure is minimal and it is possible to use strain gauge with compact dimensions for such applications. After the tests conducted with 5 specimens without the strain gauges and 5 specimens with dummy inserts, which were produced on same conditions and in the same time, it was detected that the force needed to destroy the samples with the embedded inserts is around 3% with the maximum difference calculated of 8% lower comparing to the specimens with the embedded dummy inserts.

3. Mechanical behaviour of the structure under dynamic and static loads was evaluated and results recorded and analysed. The strain measurement was defined as main mechanical property to quantify and to the log the data obtained. Main package of test were performed with two main samples, which differ only in the position of strain gauge, for first one the strain gauge is mounted on top of the structure, for the second one with the strain gauge embedded in the middle of the structure. Most of strain measurement was performed under the following conditions: strain up to 0,3% of length, with the speed of 2mm per minute and one strain run was performed under the condition of strain up to 0,5% of length, with the speed of 5mm per minute. Based on the quantified data it is seen that the difference between the strain gauge data and optical extensometer results are from 0,016 till 0,043 of strain when the sensor is mounted on top of the specimen When it comes to the specimen with fully embedded strain gauge the strain measurement the difference

from 0,029 till 0,038. This gives good indication that economically beneficial system gives small deviation from the reference.

4. Labour and equipment cost calculations were completed and presented, as seen for the data, depending on the level of accuracy several options for data acquisition systems are available. In order to measure in high precision the professional level equipment should be used, but need to keep in mind the cost differences up to 5000,00€ As a recommendation it can be to run the tests of produced samples with high accuracy data acquisition systems to record data and compare to the presented.

List of References

1. NAGHDI, Tina and ARDALAN, Sina and ADIB, Zeinab Asghari and SHARIFI, Amir Reza and GOLMOHAMMADI, Hamed. Biosensors and Bioelectronics, *Biosensors and Bioelectronics*, p. 223. 2023.
2. JANDYAL, Anketa and CHATURVEDI, Ikshita and WAZIR, Ishika and RAINA, Ankush and UL HA, Mir Irfan. 3D printing - A review of processes, materials and applications in industry 4.0. 2021.
3. HUNDE, Bonsa Regassa and WOLDEYOHANNES, Abraham Debebe. 3D printing and solar cell fabrication methods: A review of challenges, opportunities, and future prospects. *Results in Optics*. 2023.
4. Namjoshi, Janhavi and Rawat, Manish. Role of smart manufacturing in industry 4.0. *Materials Today: Proceedings*. 2022.
5. . CHO, Hyung Rok and ROH, Tae Suk and SHIM, Kyu Won and KIM, Yong Oock and LEW, Dae Hyun and YUN, In Sik. Skull Reconstruction with Custom Made Three Dimensional Titanium Implant. *Archives of Craniofacial Surgery*. 2015.
6. REN, Jun and WU, Fan and SHANG, Erwei and LI, Dongya and LIU, Yu. 3D printed smart elastomeric foam with force sensing and its integration with robotic gripper. *Sensors and Actuators: A. Physical* .2023
7. NGUYEN, Van Quyet and CHIANG, Chia-Chin and LE, Hoang-Dang and TSAI, Liren. Fabrication and testing of FBG sensor-based one-dimensional shock accelerometer attached to novel 3D printed structure . *Optik* . 2023.
8. STANOA, Gianni and DI NISIOB Attilio and LANZOLLAB Annamaria and PERCOCOA Gianluca. Additive manufacturing and characterization of a load cell with embedded strain gauges. Precision Engineering, 2020.
9. MUNGHEN, Doug and IACOBELLIS, Vincent and BEHDINAN, Kamran. Incorporation of fiber Bragg grating sensors in additive manufactured Acrylonitrile butadiene styrene for strain monitoring during fatigue loading. *International Journal of Fatigue*. 152, 2022.
10. FBGS Technologies GmbH. Technology: FBG Principle. Web site available from: https://fbgs.com/technology/fbg-principle/. [Viewed: 2023-03-05].
11. C.S. SHIN, C.C. CHIANG. Fatigue damage monitoring in polymeric composites using Fatigue damage monitoring in polymeric composites using. *International Journal of Fatigue*, 2006.
12. PHERO, Timothy L. and NOVICH, Kaelee A. and C. JOHNSON, Benjamin and D. MCMURTREY, Michael. Additively manufactured strain sensors for in-pile applications. *Sensors and Actuators: A. Physical,* 2022.
13. Electrochemical solutions. Micruxfluidic. Web site available from: https://www.micruxfluidic.com/en/electrochemical-solutions/thin-film-electrochemical-sensors/interdigitated-electrodes-ide/. [Viewed: 2023-03-05].
14. Strain shielding in distal femur after patellofemoral arthroplasty under different activity conditions. Web site available from:https://pubmed.ncbi.nlm.nih.gov/20004900/#:~:text=Strain%20shielding%2C%20a%20m echanical%20effect,which%20can%20promote%20implant%20loosening. [Viewed: 2023-03-05].YAN, Wen and MA, Shengran and HONGZHI, Wang and ZHANG, Xinpu. Fiber Bragg grating online packaging technology based on 3D printing. *Optics and Laser Technology*. 2020
15. Strain_gauge_meas.pdf. Web site available from: http://elektron.pol.lublin.pl/elekp/ap_notes/ni_an078_strain_gauge_meas.pdf. [Viewed: 2023-02-02].
16. Elprocus. Elprocus. Web site available from: https://www.elprocus.com/types-of-strain-gauge/. [Viewed: 2023-04-04].

17. Wheatstone Bridge Circuit. HBM. Web site available from: https://www.hbm.com/en/7163/wheatstone-bridge-circuit/. [Viewed: 2023-02-02].
18. The Strain Gauge. Omega. Web site available from: https://www.omega.co.uk/literature/transactions/volume3/strain3.html#:~:text=Apparent%20strain%20is%20any%20change,gage%20and%20the%20test%20specimen. [Viewed: 2023-03-03].
19. Properties, ISO 527 Plastics - Determination of tensile. Web site available from: https://view.elaba.lt/standartai/view?search_from=primo&id=863251. [Viewed: 2023-03-03].
20. Kaunas Technology University. MIDF. Tinius Olsen H25KT. Web site available from: https://apcis.ktu.edu/MIDF/lt/site/katalogas?more=9357. [Viewed: 2023-03-02].
21. Tinus Olsen. VEM 300 SERIES. Web site available from: Tinus Olsen. https://www.tiniusolsen.com/product/vem-300-series/. [Viewed: 2023-03-03].
22. Data Acquisition System DAQ/DAS. Analog. Web site available from: https://www.analog.com/en/design-center/glossary/data-acquisition-system-daq-das.html#:~:text=A%20data%20acquisition%20system%20(or,or%20by%20a%20standalone%20device. [Viewed: 2023-05-03].
23. Arduino. Web site available from: https://store.arduino.cc/products/arduino-uno-rev3. [Viewed: 2023-04-03].
24. TINYTRONICS. Load Cell Amplifier- HX711. Web site available from: https://www.tinytronics.nl/shop/en/sensors/weight-pressure-force/load-cells/load-cell-amplifier-hx711. [Viewed: 2023-02-02].
25. ELECTRONICS COACH. Wheatstone bridge. Web site available from: https://electronicscoach.com/wheatstone-bridge.html. [Viewed: 2023-04-05].
26. THE BRITANNICA DICTIONARY. The Britannica Dictionary. Sample, 2023. Web site available from: https://www.britannica.com/dictionary/sample. [Viewed: 2023-03-01].
27. PRUSA 3D. PLA. Prusa 3D. Web site available from: https://help.prusa3d.com/article/pla_2062. . [Viewed: 2023-01-01].
28. PRUSA. Original Prusa i3 MK3S+ 3D printer. Prusa. Web site available from: https://www.prusa3d.com/product/original-prusa-i3-mk3s-3d-printer-3/. [Viewed: 2023-01-15].
29. FARNELL. PPC221. Farnell. Web site available from: https://fi.farnell.com/en-FI/pro-power/ppc221/antistatic-tape-pi-film-33m-x/dp/2061300. . [Viewed: 2023-02-01].
30. FLYABILITY SA. Visual inspections: a complete guide. Web site available from: https://www.flyability.com/visual-inspection. . [Viewed: 2023-03-03].
31. HBM. B2B store by HBM. Web site available from: https://b2bstore.hbm.com/myHBM/app/displayApp/(cpgnum=1&layout=7.01-16_153_6_9_70_34_65_73_134_6&uiarea=6&citem=233A0A4E6721194EE1000000AC1099340017A47744441ED2A5BE1FFDD1C96CB6&carea=233A0A4E6721194EE1000000AC109934&xcm=hbm_b2boccasionalcrm&rdb=0&cpgsize=.[Viewed: 2023-02-03].
32. NATIONAL INSTRUMENTS CORP. Cdaq V1101. Web site available from: https://www.ni.com/sv-se/shop/model/cdaq-v1101-bundle.html. [Viewed: 2023-05-01].
33. ANODAS. Arduino Uno R3. Web site available from: https://www.anodas.lt/en/arduino-uno-r3. [Viewed: 2023-03-14].
34. ANODAS. HX711 Load Cell Module. Web site available from: https://www.anodas.lt/en/hx711-load-cell-module?search=load%20cell. [Viewed: 2023-03-15].
35. LIETUVOS OFICIALIOSIOS STATISTIKOS PORTALAS. Darbo užmokestis šalyje. Web site available from: https://osp.stat.gov.lt/informaciniai-pranesimai?articleId=10665258. [Viewed: 2023-02-01].
36. VEM 300 SERIES. Tinius Olsen. Web site available from: https://www.tiniusolsen.com/product/vem-300-series/. [Viewed: 2023-04-06].

Appendices

Appendix 1. Data sheet of 1-LM11-6/350GE strain gauge

HBM — an HBK company

Dehnungsmessstreifen
Strain gages
Jauges d'extensométrie

|	
Bestellnummer / Order No. / No. de référence	**1-LM11-6/350GE**
Typ / Type / Type	6/350GE LM11
Widerstand / Resistance / Résistance	350 Ω ±0.30 %
Stückzahl / Contents / Quantité	10
k-Faktor / Gage factor / Facteur k	2.08 ±1.0 %
Temperaturkoeffizient des k-Faktors / Temperature coefficient of gage factor / Coefficient de température du facteur k	-302 ±10 [10^{-6} / K]
Querempfindlichkeit / Transverse sensitivity / Sensibilité transverse	-4.5 %
Folienlos / Foil lot / Lot de la feuille	A558/01/02
Herstellungslos / Production batch / Lot de fabrication	812105426

Temperaturkompensation: Ferritischer Stahl mit
Temperature compensation: steel with
Compensation de température: acier avec
$\alpha = 10.8$ [10^{-6} / K]

Max. effekt. Brückenspeisespannung
max. rms bridge excitation voltage
tension d'alim. de pont maxi eff.
14.0 V

RoHS ✓
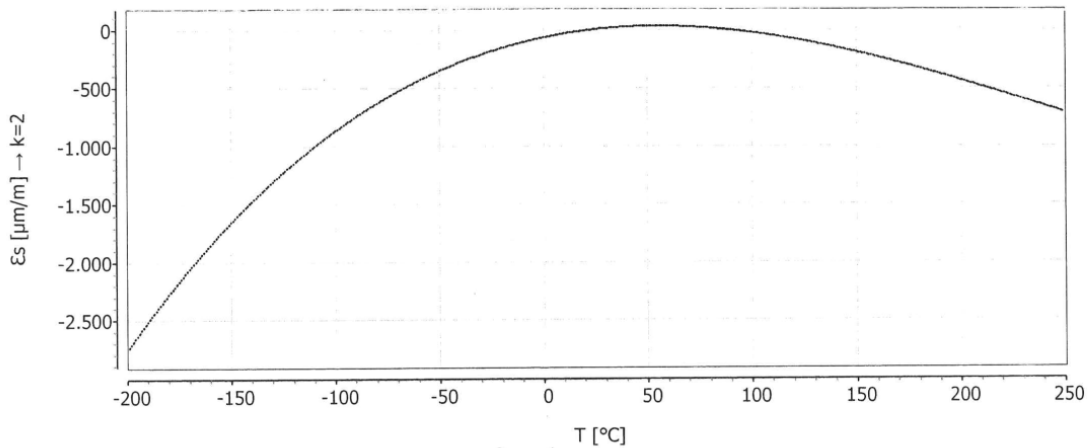
Curve 1

$$\varepsilon_S(T) = -63.40 + 3.70 * T - 3.82E\text{-}02 * T^2 + 5.28E\text{-}05 * T^3 - 2.85E\text{-}09 * T^4 \pm (T\text{-}20) * 0.60 \text{ [µm/m]}$$

Alle technischen Daten nach VDI/VDE 2635. Geben Sie bei Rückfragen bitte Bestellnummer und Herstellungslos an.

All specifications in accordance with VDI/VDE 2635. In case of further inquiries please indicate order no. and production batch number.

Toutes les caractéristiques techniques selon la norme VDI/VDE 2635. Dans toutes communications, prière d'indiquer le numéro de commande et le numéro du lot de production.

Réponse en température des jauges d'extensométrie appliquées sur des matériaux dont des coefficients de dilatation termique α sont indiqués. Mesurée à variation continue de la température.

Courbe 1: Jauges sans pattes de raccordement.
T = température en °C
(sans dimension)

Temperaturgang der Dehnungsmessstreifen bei Applikationen mit oben angegebenen Wärmeausdehnungskoeffizienten α. Gemessen bei kontinuierlicher Temperaturänderung.

Kennlinie 1: DMS ohne Anschlussbändchen.
T = Temperatur in °C
(dimensionslos)

The **temperature response** refers to strain gages bonded to materials with specified coefficients of thermal expansion α. Values are measured with continuous temperature variation.

Curve 1: Strain gages without leads.
T = temperature in °C
(dimensionless)

Kopfdaten / Header / Titre

Das Polynom für den Temperaturgang wurde bis 250°C gemessen. Für den erweiterten Einsatzbereich bis 300°C kann das Polynom annähernd extrapoliert werden.

The polynomial for the temperature response was measured up to 250 °C. The polynomial for the extended operating range up to 300 °C can be approximately extrapolated.

Le polynôme pour la réponse en température a été mesuré jusqu'à 250 °C. Le polynôme pour la plage étendue d'utilisation jusqu'à 300 °C peut être approximativement extrapolé.

A point (".") is used as decimal separator in data; the separator needs to be configured accordingly for import into Excel.

Appendix 2. Information sheet of 1-LS5_5 soldering points

**Lötstützpunkte
Solder Tags
Cosses-relais**

HBM
an **HBK** company

Bestellnummer Order. No. No. De réference	**1-LS5_S**	Herstellungslos Production batch Lot de fabrication	**812045875**

Typ
Type
Type

LS5_S

Stückzahl
Contents
Quantité

125

Paar
pairs
paires

Selbstklebend - Lagerfähigkeit bei Raumtemperatur max. 12 Monate ab Auslieferung
Temperaturbereich: -200...+180°C, kurzzeitig +260°C

Self-sticking - Shelf life at room temperature max. 12 months from delivery
Temperature range: -200...+180°C [-328°F...+356°F], short term +260°C [500°F]

Auto-collant - Durée de vie à la température ambiante max. 12 mois après la livraison
Plage de temperature: -200...+180°C, temporairement +260°C

Appendix 3. Arduino software code

```
/*
Arduino pin 2 -> HX711 CLK
 3 -> DAT
 5V -> VCC
 GND -> GND

#include "HX711.h"


#define DOUT  3
#define CLK  2
HX711 scale;

void setup() {
  Serial.begin(9600);
  Serial.println("HX711 scale demo");
  scale.begin(DOUT, CLK);
  scale.set_scale(calibration_factor);
  scale.tare();
  Serial.println("Readings:");
}
void loop() {
  /*Serial.print("Reading: "); */
 // Serial.println("units");
 // Serial.print(scale.get_units(), 2); //scale.get_units() returns a float
 // Serial.println("\n");
  uint8_t gain = scale.get_gain();
//  Serial.println("gain");
//  Serial.println (gain);
// Serial.println("\n");
  float discrete_value = scale.get_value();
  float rez = 350;
 // float pad_itampa = 5;
  float pad_itampa = 4.07;
    //float gr_itampa = ((discrete_value / 16777216) * pad_itampa) / gain;
  float gr_itampa = (discrete_value / 16777216) * pad_itampa / gain;
  //24bit max value equals 2^24 (16777216) equals 5V
  //discrete_value equals some volts
  //voltage equals = discrete_value * 5V / 16777216
// Serial.println("voltage");
//Serial.println("\n");
//Serial.print(scale.get_value(), 2); //scale.get_units() returns a float
//*Serial.print(" lbs"); //You can change this to kg but you'll need to refactor the calibration_factor */
```

```
//float Rx_varza = (((rez * rez) + rez * (rez + rez)) * (gr_itampa / pad_itampa)) / (((rez -(rez + rez))
* (gr_itampa / pad_itampa)));
  float Rx_varza = (122500 + 350 * 700 * (gr_itampa / pad_itampa)) / (350 -700 * (gr_itampa /
pad_itampa));
float V_out = pad_itampa * ((Rx_varza/(rez+Rx_varza))-(rez/(rez+rez)));
float strain = (((Rx_varza-350)/Rx_varza)/2.08);
float strain2 = ((4/2.08)*(gr_itampa/pad_itampa));
Serial.print (gr_itampa, 10);
Serial.print(",");
Serial.print (Rx_varza, 5);
Serial.print(",");
Serial.print (strain, 5);
Serial.print(",");
Serial.print (strain2, 5);
Serial.print ("\n");
//Serial.println("V_out");
//Serial.println(V_out, 8);
//Serial.println("Resistance");
//Serial.println (Rx_varza, 5);
//Serial.println("\n");
//Serial.println();
  delay (50);
}
```

Appendix 4. Prusa PLA material datasheet

Version: 1.0
Last update: 20-09-2018

PRUSA POLYMERS
by JOSEF PRUSA

TECHNICAL DATA SHEET

Prusament PLA by Prusa Polymers

PLA is the most commonly used filament. It's biodegradable, easy to print, and very strong.
The perfect choice for printing large objects thanks to its low thermal expansion (little to no warping)
and for printing tiny parts because of its low melting temperature.

APPLICATIONS:
Concept models, functional prototypes, low-wear toys, etc.

NOT SUITABLE FOR:
Long term outdoor usage because of low temperature resistance (up to 60 °C).

POST-PROCESSING:
Wet sanding. Without water you'll quickly start heating the plastic by friction, it will melt locally and
make it hard to keep sanding.

IDENTIFICATION:

Trade name	Prusament PLA
Chemical name	Polylactic Acid
Usage	FDM 3D printing
Manufacturer	Prusa Polymers, Prague, Czech Republic

RECOMMENDED PRINT SETTINGS:

Nozzle Temperature [°C]	210 ± 10
Heatbed Temperature [°C]	40–60
Print Speed [mm/s]	up to 200

TYPICAL MATERIAL PROPERTIES:

| Physical Properties	Typical Value	Method
Peak Melt Temperature [°C]	145-160	ISO 11357
Glass Transition Temperature [°C]	55-60	ISO 11357
MFR [g/10min][1]	10.4	ISO 1133
MVR [cm³/10min][1]	9.4	ISO 1133
Specific Gravity [g/cm³]	1.24	ISO 1183
Moisture Absorption 24 hours [%][2]	0.3	Prusa Polymers
Moisture Absorption 7 days [%][2]	0.3	Prusa Polymers
Moisture Absorption 4 weeks [%][2]	0.3	Prusa Polymers
Heat Deflection Temperature (0,45 MPa) [°C]	55	ISO 75
Tensile Yield Strength Filament [MPa]	57.4 ± 0.4	ISO 527-1

[1] 2,16 kg; 210 °C | [2] 28 °C; humidity 37 %

MECHANICAL PROPERTIES OF PRINTED TESTING SPECIMENS[3]:

Property / print direction	Horizontal	Vertical X,Y-Axis	Vertical Z-Axis	Method
Tensile Modulus [GPa]	2,2 ± 0,1	2,4 ± 0,1	2,3 ± 0,1	ISO 527-1
Tensile Yield Strength [MPa]	50,8 ± 2,4	59,3 ± 1,9	37,6 ± 4,0	ISO 527-1
Elongation at Yield Point [%]	2,9 ± 0,3	3,2 ± 0,1	1,9 ± 0,3	ISO 527-1
Impact Strength Charpy[4] [kJ/m²]	12,7 ± 0,7	13,7 ± 0,7	5,0 ± 1,4	ISO 179-1

[3] Original Prusa i3 MK3 3D printer was used to print testing specimens. Slic3r Prusa Edition 1.40.0 was used to create G-codes with following settings: Prusa PLA Filament; Print settings 0,20mm FAST (layers 0,2mm); solid layers Top: 0 Bottom: 0; Infill 100% Rectilinear, infill print speed 200mm/s; extruder temperature 215°C all layers; bed temperature 60°C all layers; other parameters set to default | [4] Charpy Unnotched, edgewise direction of blow according to ISO 179-1

DISCLAIMER

The results presented in this data sheet are just for your information and comparison. Values are significantly dependent on print settings, operators experiences and surrounding conditions. Everyone have to consider suitability and possible consequences of printed parts usage. Prusa Polymers can not carry any responsibility for injures or any loss caused by using of Prusa Polymers material.

VERTICAL X,Y-AXIS

VERTICAL Z-AXIS

HORIZONTAL
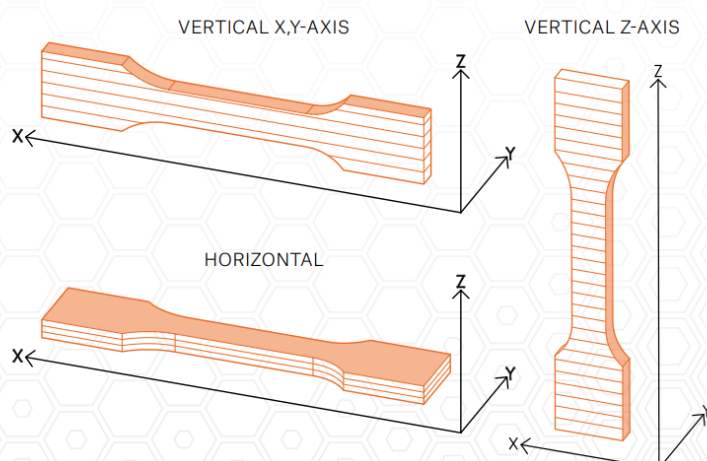
Appendix 5. Electromagnet KK-P40/20 information sheet

Electromagnet 12V 4.8W - 30kg

Product Code: ABC-16214

Availability: Vilnius Store Out of Stock

Kaunas Store In Stock

Central Warehouse Out of Stock

26.00€

Ex Tax: 21.49€

− 1 + 🛒 **Add to Cart**

♡ Add to Wish List

💬 **Description**   🚚 Product Delivery

The holding electromagnet powered with voltage of 12 V and a capacity of 4,8 W. It holds a weight of 30 kg in standard earth acceleration 9.8 m/s2. The body diameter is 40 mm and its height 20 mm, hole with M5 thread is used for mounting.

Technical data:
- Supply voltage: 12V
- Power: 4,8W
- Current consumption: approx. 400mA
- Body diameter: 40mm
- Height of the body: 20mm
- The diameter of the attraction part: 18mm
- Load capacity: 30 kg
- Mounting hole with M5 thread

Appendix 6. Prusa i3 MK3S+ 3D printer datasheet

Technical Parameters

Build Volume	25×21×21 cm (9.84"×8.3"×8.3")
Layer height	0.05 - 0.35 mm
Nozzle	0.4mm default, wide range of other diameters/nozzles supported
Filament diameter	1.75 mm
Supported materials	Wide range of thermoplastics, including PLA, PETG, ASA, ABS, PC (Polycarbonate), CPE, PVA/BVOH, PVB, HIPS, PP (Polypropylene), Flex, nGen, Nylon, Carbon filled, Woodfill and other filled materials.
Max travel speed	200+ mm/s
Max nozzle temperature	300 °C / 572 °F
Max heatbed temperature	120 °C / 248 °F
Extruder	Direct Drive, Bondtech gears, E3D V6 hotend
Print surface	Removable magnetic steel sheets(*) with different surface finishes, heatbed with cold corners compensation
Printer dimensions (without spool)	7 kg, 500×550×400 mm; 19.6×21.6×15.7 in (X×Y×Z)
Power consumption	PLA settings: 80W / ABS settings: 120W

* Consumable parts, such as print sheets (smooth, textured, etc.), are not covered by the warranty since their coatings are expected to deteriorate over time, unless the failure is due to a defect in materials or workmanship. Cosmetic damage, which includes, but is not limited to, scratches, dents, cracks, or other aesthetic damage, is also not covered. Only sheets defective upon delivery are covered by the warranty.

Appendix 7. Vishay PTF56350 data sheet

PTF

Vishay Dale

Metal Film Resistors, Axial, High Precision, High Stability

FEATURES
- Extremely low temperature coefficient of resistance
- Very low noise and voltage coefficient
- Very good high frequency characteristics
- Can replace wirewound bobbins
- Proprietary epoxy coating provides superior moisture protection
- For surface mount product, see Vishay Dale's PSF datasheet (www.vishay.com/doc?30162)
- Material categorization: for definitions of compliance please see www.vishay.com/doc?99912

Note
* This datasheet provides information about parts that are RoHS-compliant and / or parts that are non-RoHS-compliant. For example, parts with lead (Pb) terminations are not RoHS-compliant. Please see the information / tables in this datasheet for details.

STANDARD ELECTRICAL SPECIFICATIONS

GLOBAL MODEL	HISTORICAL MODEL	POWER RATING [3] $P_{85\,°C}$ W	LIMITING ELEMENT VOLTAGE MAX. [1] V	TEMPERATURE COEFFICIENT ± ppm/°C	TOLERANCE ± %	RESISTANCE RANGE Ω
PTF51	PTF-51	0.05	200	5, 10, 15	0.02, 0.05, 0.1, 0.25, 0.5, 1	15 to 100K
PTF56	PTF-56	0.125	300	5, 10, 15	0.01, 0.02, 0.05, 0.1, 0.25, 0.5, 1	15 to 500K
PTF65	PTF-65	0.25	500	5, 10, 15	0.05, 0.1, 0.25, 0.5, 1	15 to 1M

Notes
- DSCC has created a drawing to support the need for a precision axial-leaded product. Vishay Dale is listed as a resource on this drawing as follows:

DSCC DRAWING NUMBER	VISHAY DALE MODEL	POWER RATING $P_{85\,°C}$ W	RESISTANCE RANGE Ω	TOLERANCE ± %	TEMPERATURE COEFFICIENT ± ppm/°C	MAXIMUM WORKING VOLTAGE [1] V
89088	PTF56..31, PTF56..32 [2]	0.100	15 to 100K	0.01, 0.05, 0.1, 0.5, 1	5, 10	200
90038	PTF65..16, PTF65..14 [2]	0.250	15 to 100K	0.05, 0.1, 0.5, 1	5, 10	200

This drawing can be viewed at: www.landandmaritime.dla.mil/Programs/MilSpec/ListDwgs.aspx?DocTYPE=DSCCdwg
[1] Continuous working voltage shall be $\sqrt{P}$ x R or maximum working voltage, whichever is less.
[2] Hot solder dipped leads.
[3] For operation of the PTF resistors at higher power ratings, see the Load Life Shift Due to Power and Derating table. This table gives a summary of the effects of using the PTF product at the more common combinations of power rating and case size, as well as quantifies the load life stability under those conditions.

TEMPERATURE COEFFICIENT CODES

GLOBAL TC CODE	HISTORICAL TC CODE	TEMPERATURE COEFFICIENT
Z	T-16	5 ppm/°C
Y	T-13	10 ppm/°C
X	T-10	15 ppm/°C

GLOBAL PART NUMBER INFORMATION

New Global Part Numbering: PTF5620K500BYRE (preferred part numbering format)

| P | T | F | 5 | 6 | 2 | 0 | K | 5 | 0 | 0 | B | Y | R | E | | | |

GLOBAL MODEL	RESISTANCE VALUE	TOLERANCE CODE	TEMP. COEFFICIENT	PACKAGING	SPECIAL
PTF51 PTF56 PTF65	R = Ω K = kΩ M = MΩ 15R000 = 15 Ω 500K00 = 500 kΩ 1M0000 = 1.0 MΩ	T = ± 0.01 % [1] Q = ± 0.02 % [1] A = ± 0.05 % B = ± 0.1 % C = ± 0.25 % D = ± 0.5 % F = ± 1 %	Z = 5 ppm Y = 10 ppm X = 15 ppm 0 = special	EK = lead (Pb)-free, bulk EA = lead (Pb)-free, T/R (full) EB = lead (Pb)-free, T/R (1000 pieces) BF = tin/lead, bulk RE = tin/lead, T/R (full) R6 = tin/lead, T/R (1000 pieces)	Blank = standard (Dash number) (Up to 3 digits) From 1 to 999 as applicable

Historical Part Number example: PTF-5620K5BT-13R36 (will continue to be accepted)

PTF-56	20K5	B	T-13	R36
HISTORICAL MODEL	RESISTANCE VALUE	TOLERANCE CODE	TEMP. COEFFICIENT	PACKAGING

Notes
- For additional information on packaging, refer to the Through-Hole Resistor Packaging document (www.vishay.com/doc?31544).
[1] Historical tolerance codes were BB for 0.01 % and BC for 0.02 %.